Catena 215 (2022) 106312

Contents lists available at ScienceDirect

Catena

journal homepage: www.elsevier.com/locate/catena

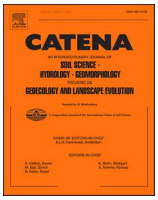

Footpaths: Pedogenic and geomorphological long-term effects of human trampling

Nadav Nir [a,*], Mareike Stahlschmidt [b], Robert Busch [a], Christopher Lüthgens [c], Brigitta Schütt [a], Jacob Hardt [a]

[a] Institute of Geographical Sciences, Freie Universität Berlin, Berlin, Germany
[b] Department of Human Evolution, Max Plank Institute for Evolutionary Anthropology, Leipzig, Germany
[c] Vienna Laboratory for Luminescence Dating, University of Natural Resources and Life Sciences (BOKU), Vienna, Austria

ARTICLE INFO

Keywords:
Footpaths
Gully erosion
Sunken lanes
Micromorphology
Porosity
Pedogenic iron
Soil development
Human imapct
Trails

ABSTRACT

Footpaths are of the oldest and most widely distributed forms of human imprint on the landscape. These elongated features are the result of continuous usage of a certain route for walking, at time scales ranging from days to centuries or millennia. In this qualitative investigation, we take a holistic approach combining micromorphology (including voids analysis), chemical soil parameters (such as selective iron oxide dissolution), and remote sensing (spatial distribution and orientation of footpaths in the landscape) to evaluate the long-term residues and environmental effects resulting from the formation of footpaths. Our diverse case studies incorporate footpaths used for recreational and transport purposes in temperate and sub-humid climates from both recent and historical perspectives. A reduction of the large pores was observed down to 3 cm below current and historical surfaces compared to control areas without footpaths. The lower porosity subsequently hinders of the supply of oxygen and/or water into the sub-surface and encourages water stagnation on the compacted footpath surface. These processes result in higher amounts of pedogenic Fe oxides and, at times, macro-organic residues under footpaths and hindering of soil formation. As an additional result of compaction, surface runoff is promoted. The latter may either trigger the initiation of gullies directly downslope from footpaths or lead to incision of the footpaths themselves. Incised footpaths are more likely to occur when the footpath is oriented parallel to the stream network. Once an incised footpath is formed, it may reduce gully erosion susceptibility downslope as the incised footpath acts as a channel that decreases a footpath's 'overbank' flow. With a better understanding of footpaths as landscape units we can (1) pose archaeological questions related to human environmental interaction, (2) assess carbon storage potential under footpaths and (3) use incised footpaths as possible measures against gully erosion.

1. Introduction

Humans have historically affected and continue to have an effect on soil formation, erosion and degradation (Butzer, 2005; Storozum et al., 2021). Historical changes in land cover triggered by land use requirements, such as the removal of natural vegetation and its replacement with agricultural crops, have shown to promote soil erosion as early as the first millennia BCE (van Andel et al., 1990). A special type of land cover that has dominated areas used by humans are footpaths. In the Near East, the latter have been evident at least since the early Bronze age (Snead et al., 2009). Pathways have been intensely investigated in archaeological contexts from a route network perspective, with a growing use of remote sensing techniques (Verhagen et al., 2019), with few exceptions (Wilkinson et al., 2010). Since the time of road construction and usage of pavements, pathways are considered as archaeological features (Zedeño and Stoffle, 2003). However, footpaths, the unconstructed and unwheeled predecessors of paved pathways and roads, might have influenced the landscape far before the Bronze age. Although spatially and temporally widely distributed, footpaths as a human-landscape feature have gained little attention in the archaeological research with few exceptions (Snead et al., 2009). Recreational trails having been investigated for their possible effect on vegetation cover and soil erosion. However, data remains scarce, distinctions between wheeled and non-wheeled paths are inconsistent, and little is

* Corresponding author.
E-mail address: nadavnnir@gmail.com (N. Nir).

https://doi.org/10.1016/j.catena.2022.106312
Received 4 October 2021; Received in revised form 31 March 2022; Accepted 14 April 2022
Available online 5 May 2022

known on footpath's relationship with soil formation or the drainage basin dynamics (Sidle et al., 2019; Wimpey and Marion, 2010; Buchwał and Rogowski, 2010; Cole, 2004).

1.1. Trampling and soil compaction

The process of modifying surfaces and sub-surfaces as a consequence of repeated human and animal movement is usually referred to as "trampling". Human trampling has long been in the focus of micro-archaeological investigations (Rentzel et al., 2017). Micromorphological experiments and investigations of archaeological records suggest that the structure of sediments, soils and human residues is affected by trampling. This is expressed by texture characters such as the breakage of bones and ash layers and the general compaction of archaeological materials. In soils, indications of trampling can be platy microstructures and horizontal to polyconcave voids and reduction of overall porosity (Miller et al., 2010; Goldberg and Berna, 2010; Rentzel et al., 2017). For organic components, it is suggested that trampling re-organizes plant fibres originating from dung, resulting in a sub-parallel platy macro-structure (Shahack-Gross et al., 2003). Additionally, complex packing voids, a lack of void structures and massive microstructures were evident in different open areas occupied by humans and cattle (Pietola et al., 2005). The pressures adult humans can induce on the underlying ground depends on their static versus moving positioning. The range incorporating both, standing and moving, lies between 60 and 500 kPa (Asmi et al. 2020; Rodgers, 1988). Bernhardt-Römermann et al. (2011) concluded for 35 trails in European forests, that historical human land use and local climate strongly affected the resilience and resistance of plants to human trampling and that this process differs for different environments (Bernhardt-Römermann et al. 2011). Agricultural soils have long been investigated for the effect of compaction due to heavy machinery (Coulon and Bruand, 1989). Few of these studies have used micromorphology as a tool to understand the effect pressure has on the sub-soil. Results show that changes in voids' structure reach well into the first centimetres of the soil. It has been observed that vertical voids are blocked from reaching the surface - at the same time, concentrated voids are formed in the sub-soil (Rasa et al., 2012; Iraj et al., 2011). An experiment by Silva el al. (2011) studied the effects of direct pressure on soil nitrogen (N) and carbon (C) contents. For pressure levels up to 240 kPa, soil density increased between 20 and 22%. However, in one occasion, the rate of Total Organic Carbon (TOC) loss through mineralization decreased and TOC concentration increased starting at a pressure of 120 kPa (Silva et al., 2011). This degree of pressure is within the range applied by walking human adults and cattle. Other experiments imply that lower extents of pressure might result in higher Total Carbon (TC) and Total Nitrogen (TN) compared to those induced by heavy compaction (Blumfield et al., 2005; Wang et al., 2020). Some authors explain the changes in TOC and N concentration as the result of changes in the density of both macro- and micro-porosity of the soil which in turn affects microbial activity, mostly through the supply of oxygen and the degree of photosynthesis (Neve and Hofman, 2000; Silva et al., 2011). Following this notion, it has been found that a large portion of soil organic matter (SOM) is stabilized within the entrance of small pores (Kawahigashi et al., 2006; Kaiser et al., 2002). It was subsequently suggested that reducing porosity and therefore microbial activity affects C and N cycling (Mikutta et al., 2006). Further experimental work found that SOM stability is affected by the changes in aggregate types and heavy compaction (Silva et al., 2011; Guimarães et al., 2013; Mikutta et al., 2006). The carbon mineralization rate decreases as bulk densities increase, up to some extent of pressure, indicating that carbon mineralization in moderately compacted soils can lead to an increase in the accumulation of organic matter (Neve and Hofman, 2000). Additionally, identifying changes in the relative amounts of poorly crystalized pedogenic iron oxides serves as an indicator for long-term residues of compaction as they are affected by water and air availability and relate to organic matter decomposition (Chen et al., 2020; Coward et al., 2017). Experimental works and investigations looking into vegetation response to trampling have shown that compaction by human induced pressure may decrease biomass and increase soil density especially in the upper 5 cm of the soil but might also reach down as far as 20 cm (Sherman et al., 2019). Soil moisture and organic matter have shown a mixed reaction to pressure while soil pH has slightly increased in soils under footpaths (Kissling et al., 2009; Sherman et al., 2019). To date, no micromorphological or selective Fe extraction studies have directly addressed the formation of footpaths. Recreational tracks and footpaths studies were focused predominantly on vegetation cover and on aspects of soil erosion (Sherman et al., 2019; Ayres et al., 2008; Cole, 2004).

1.2. Gully erosion and pathways

Soil erosion has been correlated with geological, topographic, climatic and human induced variables (Addisie et al., 2018; Vandaele et al., 1996; Valentin et al., 2005). One point of origin for soil erosion are roads and pathways. Due to the high compaction of their surfaces, runoff generation is favoured and gullies, a linear form of soil erosion exceeding 30 cm depth, can initiate downslope (Ziegler et al., 2000; Nyssen et al., 2002; Nir et al., 2021). Mostly in silty environments and presumably when a pathway is oriented down slope, a different linear erosional process may occur: the erosion and incision of the path itself, usually termed a *sunken lane* or, in historical and archaeological context named as *hollow way* (Bell and Leary, 2020). Similar to other forms of pathways, sunken lanes are seen as the result of the movement of people, animals, and different types of transport (Nir et al., 2021). The additional factor differentiating it from a pathway is the water induced mass transport, controlled by the slope angle (Boardman, 2013). The elongated and gully-like sunken lanes are usually defined as such when they are incised at least 0.5 m into the surrounding surface, a threshold related to the crossing abilities of agricultural vehicles (Geeter et al., 2020; David et al., 2011; Zgłobicki et al., 2021). The threshold for the development of sunken lanes is heavily dependent on human activities and does not necessarily require steep slopes as gullies often do. However, steeper slopes may generate deeper sunken lanes (Geeter et al., 2020). Shallow forms of sunken lanes, ca. $<$0.5 m "sunken" into the surrounding surface, are also prominent features in the landscape resulting from the incision of footpaths (Zgłobicki et al., 2021). Throughout the course of a single footpath, it can change from being levelled with its surroundings to being slightly incised (ca. $<$0.5 m) or to form a sunken lane ($>$0.5 m). During flash flood events in the non-sunken section, surface runoff may occur that in turn could trigger gully erosion in its downslope vicinity. Hence, both types of footpath-related linear erosional forms can initiate within the course of one path (Busch et al., 2021; Nir et al., 2021).

1.3. Objectives

In the present study we investigate the formation processes of footpaths as they affect and are affected by surface runoff and soil formation. We aim to determine differences and similarities between the erosion attributes when historically used footpaths are incised. We expect to find differences in the amount of voids and pedogenic Fe oxide contents in the topsoils of currently used and historical footpaths, as both are influenced by compaction and the supply of water and oxygen, and relate to each other. An initial and multi-method qualitative investigation follows a holistic approach in order to better understand the effects of human movement on top-soil characters and erosion dynamics. Using the case studies from both temperate and sub-humid zones, we examine the modern and long-term effects of footpaths formation. Our aim is to (1) recognize possible patterns and changes in the top-soil of footpaths and incision of footpaths using micromorphology, focussing on void pattern image analyses in the top-soils and selected chemical characters of the top-soils, (2) asses these patters under different climatic conditions and in different soil types, and (3) evaluate the interplay of long-

term used (and subsequently incised) footpaths with soil erosion on a drainage basin scale.

2. Case studies

The Tigray region of the Ethiopian highlands, representing a developing nation under sub-humid climate, has been intensively studied for both its gully erosion (Billi and Dramis, 2003; Busch et al., 2021; Frankl et al., 2012) and pathway systems (Nir, 2021; Nyssen et al., 2020) as well as its substantial archaeological records (Nyssen et al., 2004; Fattovich, 2010; Nyssen et al., 2020). Against this backdrop, Tigray appears as a perfect study area to conduct research into the soil properties of pathways. As a counterpoint and as a subject of comparison in a different climate zone and with completely different soil conditions, we identified three currently used recreational footpaths in different soil types under temperate climate in Germany. The selection of a number of highly diverse study sites aims to provide robust data to assess the formation of currently and long-termed used footpaths and their possible effect on landscape dynamics (Fig. 1).

The selection of the six case study sites and the slightly differing methods applied at the various locations, were chosen to identify the different environmental and temporal effects of footpath use (Fig. 2). In Germany, the currently used footpaths result from recreational use. We selected a sandy forest environment, a clayey forest environment and a loamy urban park environment. In Tigray, incised footpaths in proximity to 1st millennium BCE archaeological sites were chosen to represent a likely historical use of footpaths (Fig. 2). The two likely historical footpaths reflect long distance and daily short distance travel in clayey soils until today. Another footpath in Tigray represents modern use in an agricultural context (narrow path used by farmers between fields), although the path is located within a watershed where first millennia BCE pottery sherds were found (archaeological survey, Pfeifer et al., in press). Therefore, although most study sites share the same methodological approach, the three German case study sites are interpreted rather as currently used footpaths, while the Tigray footpaths are regarded more as long-term use indicators. Subsequently, footpaths in Germany were always micromorphologically studied from 0 cm below surface and measured for surface resistance, while in the Tigray case study sites, the focus was put on the lower 5–20 cm below surface (apart from the likely modern footpath). Additionally, the geomorphological aspect of footpaths, attributed to long term use, has been investigated by analysing remote sensing data and accompanying field surveys for the sites in Tigray.

2.1. Germany

2.1.1. Berlin footpaths

Two of the investigated footpaths are located in Berlin (Germany; Figs. 1-3), one in the Grunewald Forest (sample G1, Fig. 3) and one in an urban park in south Berlin (Gemeindepark) (sample G2, Fig. 3). The annual precipitation of the region averages 577 mm and the average annual temperature amounts 8.9 °C. The Grunewald Forest marks the western margins of Berlin. Here, sandy soils (*Haplic Arenosol*) with an organic horizon reaching up to 8 cm thickness developed in Pleistocene glaciofluvial sediments. The sampled footpath (sample G1) is situated at the margins of a ridge (100 m asl), continuing on a slope that sharply (>20°) descends west towards the River Havel. In the urban park a footpath (sample G2) was selected for sampling which is oriented semi-diagonally and at times parallel to a paved way. The urban park was constructed and opened to the public in 1912. The soils of the park developed in mixed sands and silts with cultivated lawns dominating most of the area (Wessolek et al., 2008; Umweltamt Steglitz-Zehlendorf von Berlin, 2016).

2.1.2. Ore Mountains footpath

In the Ore Mountains (Figs. 1-3) a footpath situated in a forest outside Anthonstal at the border between Germany and the Czech Republic was investigated (sample G3, Fig. 3). Podzolic and eutrophic brown earth soils are characteristic for the region while forests are characterized by short rotation pine and mature spruce forests. Annual precipitation amounts to 820–950 mm and mean air temperature is ca. 5–7.2 °C (Tichomirowa et al., 2019; Drauschke et al., 2015). The footpath is perpendicular to the slope (ca. 40°) while the bare schist bedrock is exposed at different locations directly above the footpath.

2.2. Tigray, Ethiopia

In central Tigray in the Northern Ethiopian Highlands three incised footpaths were studied. The sample names - Rama (sample R), Yeha (sample Y) and Melazo-Hawelti (sample M) - correspond to the archaeological sites in their surroundings (Fig. 4). Today's climate in Tigray is sub-humid to semi-arid and driven by the monsoon with yearly average daytime temperatures across Tigray varying from 20 °C to 35 °C. For central Tigray, the mean annual precipitation during the 20th century varied between 500 and 800 mm following a bimodal yearly pattern (Harrower et al., 2020); at times, rainfall occurs within massive storm events (Gebrehiwot and van der Veen, 2013; Berhane et al., 2020). In 2005 about 43.2% of Tigray was covered by low woodlands and shrublands while about 0.2% of the total Tigray area (~5 million ha) was covered by high woodlands and forests (FAO Forest Department, 2010). Land use today is mainly characterized by tef, wheat,

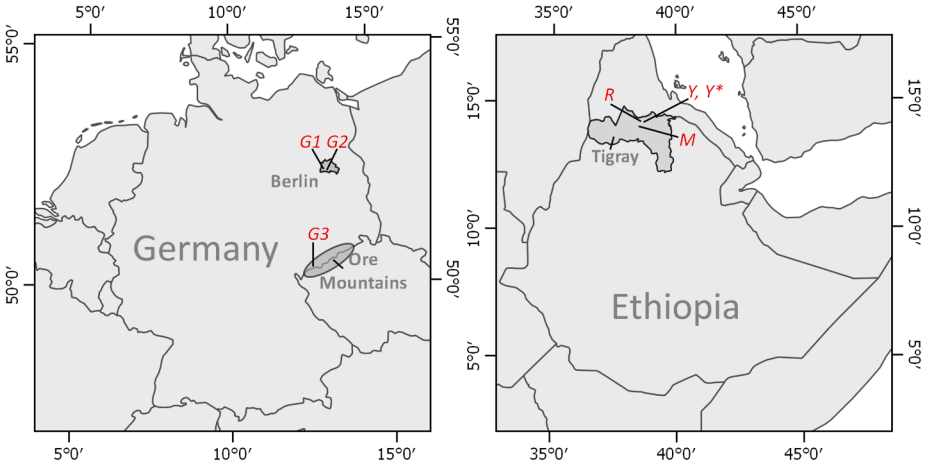

Fig. 1. Overview maps indicating the locations (marked red) of sampled footpaths from a. Germany: Grunewald Forest Berlin (G1), Urban park Berlin (G2) and Ore mountains (G3) and b. Tigray, Ethiopia: Rama (R), Yeha (Y), Yeha margins (Y*) and Melazo-Hawelti (M). Red marked G1-G3 (map a) mark overviewing the sampling locations in Germany. Natural Earth open source data available at naturalearthdata.com. (For interpretation of the references to colour in this figure legend, the reader is referred to the web version of this article.)

Fig. 2. Sampling sites on footpaths in Germany (samples G1-G3) and Tigray, sample R, sample Y, sample Y* and sample M. Red circle marks the micromorphological sampling point. (For interpretation of the references to colour in this figure legend, the reader is referred to the web version of this article.)

barley and millet cultivation (Asfaha et al., 2021). Multiple soil conservation measures have been applied to prevent soil erosion, mainly using earth bunds, furrows and grassed lynchets (locally known as *daget*). Placing stone bunds and planting of trees and bushes to stabilize larger earth bunds have been implemented since the early 1990s (Dagnew et al., 2015; Frankl et al., 2013; Nyssen et al., 2000; Nyssen et al., 2020).

Two of the oldest and most dominant archaeological sites in Tigray are the Pre-Aksumitic (early first millennium BCE) sites of Yeha and Melazo-Hawelti (Breton, 2011; Contenson, 1961). Archaeological evidence discovered in Yeha indicates almost three millennia long continuous occupation of this area including a unique and well-known temple attributed to the Ethio-Sabean material culture of the pre-Aksumite period (Weiß et al., 2016). The Melazo-Hawelti archaeological sites similarly includes a temple attributed to the Ethio-Sabean culture (Contenson, 1961; Leclant, 1959). The continuous human presence around these sites and the fact that today people still predominantly use footpaths (personal observation), make this an ideal research location. In order to identify possible older footpaths, we concentrated on the detection of incised footpaths. Three incised footpaths were selected for the current work: one selected footpath is assumed to be 'modern' (Rama incised footpath), two of the selected footpaths are incised and considered as being in historical and continuece used until today (Yeha and Melazo-Hawelti incised footpaths; Figs. 2 and 4). The mere incision of a footpath does not directly infer its age. However, the combination of their long-distance course between ancient centres, their incision, and their location within the vicinity of the pre-Aksumite archaeological sites, brought about these assumptions and selections (see Results chapter for further confirmation of the antiquity of the incised footpaths in Tigray).

2.2.1. *Rama incised footpath (sample R)*

The Rama incised footpath is situated ca. 3 km SE of the modern town of Rama (Figs. 2 and 4). Both the footpath and the town are located within a depression that covers an area approximately 3 km wide and 10 km long, striking S-N with an average elevation of 1300 m asl. The flanks of the structure are dominated by metamorphic siltstones and granitic domes; locally granitic domes also appear in the depression as isolated positive landforms while the depression is widely infilled by Quaternary sediments. Within the generally sub-humid Tigray, the micro-climate dominating the depression can reach characteristics of a semi-arid zone (Busch et al., 2021). The Rama incised footpath is considered as a modern example of a footpath that locally forms a shallow sunken lane (<0.5 m incised). The footpath starts at the eastern escarpments of the depression (at ca. 20° slope) and descends ca. 50 m into the planes, where it is disturbed and redirected by a gully and badlands. It continues through farmland until it ends in the Inda Shawit River where animals and humans cross (Busch et al., 2021). Extraction of sample R (Table 1) took place in the planes, east of the Inda Shawit River where the incised footpath is also affected by overflow of field irrigation.

2.2.2. *Yeha incised footpath (samples Y, Y*)*

The incised footpath close to the archaeological Yeha site is presumably in long-term use. It is a 16 km long north-south connection between the monastery of Mariyam Shewit and the village Ihsa'a through the modern town of Sehul (Fig. 4). The footpath runs ca. 6–9 km (varies) east of the early 1st Millennium BCE archaeological site of Yeha. The region is dominated by cone shaped hills made of volcanic plugs and domes (Machado, 2015). The footpath runs in the foot zone and in the colluvial deposits of these hills. The footpath runs parallel to a modern road, mostly perpendicular to the slope of the hills and has an inclination of ca. 5–15°. The path is used today on a daily basis by locals traveling by

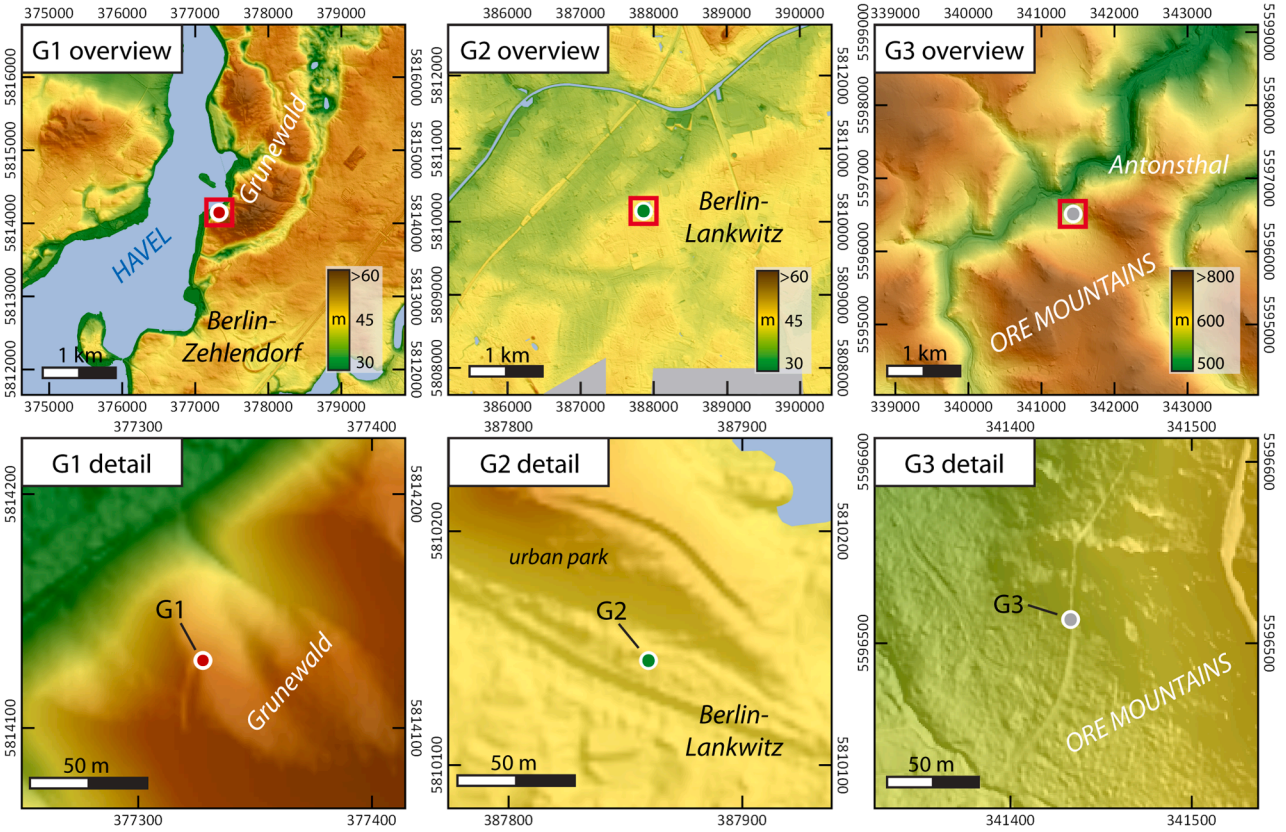

Fig. 3. Overview (top row) and detail (bottom row) maps of sampled footpaths in Germany. Coloured dots indicate the sampling sites. (Hill shade maps based on open source Lidar data (Geoportal Berlin) for G1 and G2; https://www.stadtentwicklung.berlin.de/geoinformation; and by GeoSN (GeoSN) for G3; https://www.geosn.sachsen.de).

foot or with pack animals. This footpath usually forms a shallow sunken lane (<0.5 m incised) with local incisions deeper than 0.5 m.

2.2.3. Melazo-Hawelti incised footpath (sample M)

The sampling site of the Melazo-Hawelti footpath is located where the path reaches the modern village of Hawelti in the municipality of May-Weiny (Fig. 4). The flat to hilly plateau region is composed of metamorphic sandstones and basalts (Beyth, 1972). The footpath investigated classifies as a shallow sunken lane and is located in ca. 700 m distance to the temple of Melazo. It is part of a currently daily used track from the local villages in the area towards the cities of Yeha and Adwa. The footpath has an inclination ranging between ca. 7–11°.

3. Materials and methods

A holistic multi-scale approach was selected including micro (micromorphology, sedimentary and image analyses and extraction of pedogenic Fe), meso (field description, surface resistance) and macro (remote sensing) scales, as these different scales each offer different approaches to assess the effects of footpaths on top-soil formation and erosion processes (Fig. 5).

3.1. Sampling

Micromorphological (MM) undisturbed, soil samples were extracted from the footpaths (n = 7) at a depth of 0–20 cm (Fig. 2). The Rama footpath sample (sample R) was extracted from a levelled segment of the footpath, the footpath is both-sided flanked by agricultural fields. The Yeha footpath sample (sample Y) was extracted at the centre of the footpath. A second sample from this footpath (sample Y*) was taken 1.8 km south of the first sampling Y. The sample Y* was extracted at a locality where a large boulder covers part of the footpath, acting as an obstacle for runoff and trampling; the sample was taken close to the boulder where less trampling is expected than at the central path. The Melazo-Hawelti (Melazo) footpath sample (sample M) was extracted at the centre of the footpath, where it runs through agricultural fields. Bulk material was extracted from footpath and non-footpath (control) locations from the topsoil (ca. 0–5 cm depth) and the underlying stratum (ca. 10–30 cm depth) below strata boundaries for laboratory analysis. For currently used footpaths, additional soil penetration resistance measurements using a manual penetrometer (pocket penetrometer ELE International-29–3729) were obtained to receive information on soil compaction of the soil surface; for each sampling location three replicas were measured (Tejedo et al., 2016).

For the currently used paths in Germany, a non-footpath sample (G1-3C) was taken at similar depth in ca. 1 m distance off-site of each footpath sampling location for control (n = 3). In Tigray, incised footpaths were confined by active agricultural fields characterized by ploughing and sowing activities, so that these areas were unsuitable for taking the non-footpath control samples. Therefore, the control samples used for the Tigray region reflect a landscape perspective, using several micromorphological and geochemical control samples from natural exposures (named here 'regional reference samples', n = 10). Most of the micromorphological regional reference samples were extracted from natural outcrops close to the footpath sampling locations of archaeological sites (Mussi et al., 2021). One additional reference sample from the sub-surface (5 cm below surface) was sampled from outside the Yeha incised footpath between the two sampling spots (Y and Y*); this sample was exclusively used for geochemical analysis. The micromorphological reference samples were extracted from different depths to be able to assess different pressures caused by the overburden (supplementary Table 2).

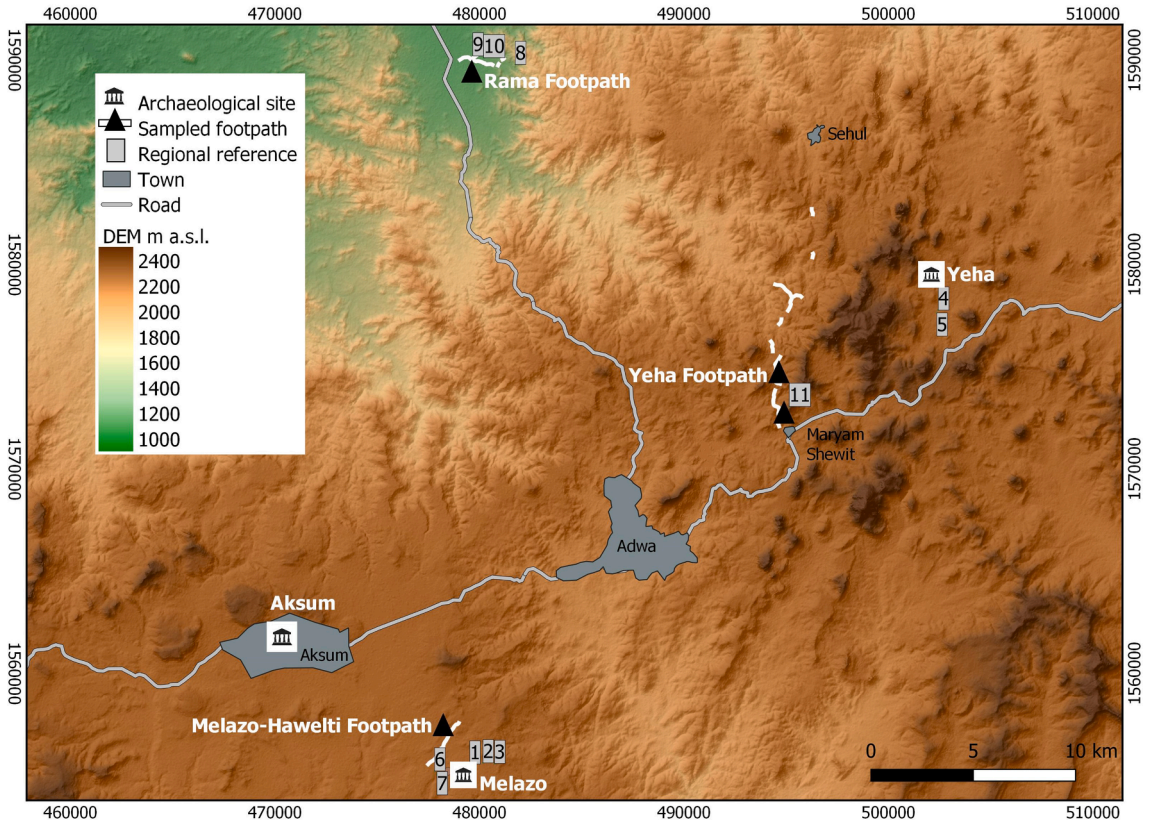

Fig. 4. Regional overview map of the study sites in Tigray, Ethiopia. White lines: One currently used incised footpath Rama (sample R), and two likely historical incised footpath; 1) Yeha samples: Y (north) and Y* (south) and 2) Melazo-Hawelti: sample M. Sampled footpaths indicated by triangles. Numbers point out the locations of regional reference samples. Elevation information based on SRTM available at USGS https://earthexplorer.usgs.gov; Jarvis et al. (2008).

3.2. Analysis

3.2.1. Micromorphological analysis

Undisturbed block samples were extracted using jackets of gypsum bandages (plaster of Paris) or plastic boxes, depending on the sediment type and cohesion. Samples were processed in the Physical Geography Laboratory of Freie Universität Berlin where they were dried for several days at room temperature (ca. 18 °C) and later heated to 40 °C for 30 h. Subsequently, sediments were impregnated using a 6:4 (v:v) mixture of polyester resin and acetone and a small amount of hardener (5–10 ml hardener to 1 l of polyester resin and acetone mixture). Due to the heavy saturation and cracking of the clay enriched sediments, acetone removal was performed and amounts and ratios were changed according to the reactions and impregnation of the sediments. After several weeks of repeated sample impregnation and drying, sampled blocks were cut with a slab saw to ca. 6x5 cm 'hand' size slabs. These units were sent for preparation of 30 μm thick sections to the Quality Thin Section labs, Arizona, with some samples completely conducted at the MKfactory labs in Stahnsdorf, Germany. Analysis of the slides was performed using four objective lenses (x2.5, x10, x20 and x40), along with x10 ocular lenses, resulting in four magnifications (x25, x100, x200 and x400) in plane and cross polarized lights (PPL and XPL) on a Zeiss polarizing microscope following common micromorphological studies (Stoops, 2021; Verrecchia, 2021).

3.3. Voids analysis

Voids quantification and measuring the extent of porosity has been used by micromorphologists for several decades (Pires et al., 2009). Here, we analysed voids at five scales according to objective lens: x2.5 (field of view: 20,200 μm), x5 (field of view: 18,500 μm), x10 (field of view: 11,100 μm), x20 (field of view: 5,700 μm) and x40 (field of view: 2,900 μm). For each of these objective lenses, pictures were taken in 1 cm steps, starting at 0.1 cm below the upper border of each slide, reaching 5 cm. Each segment in all scales was photographed in plane polarized light (PPL) and at cross polarized light (XPL). The locations chosen were at a vertical line along the horizontal centre of the slides. For the higher objective lenses (x10, x20, x40) the image was directed to a matrix area were voids fit within the objective lens frame (except for planes where these could cross the borders to some extent) to be able to analyse the 'micro-voids'. The quantification of the number of voids for each scale was conducted using R basic package in R environment (R Core Team, 2013), using 'cimg' and 'greyscale' functions for both, PPL and XPL images ('imager' package). A major task was to differentiate between quartz minerals and voids, as both appear alike in the plane polarized light. In cross polarized light the quartz minerals show a characteristic colour sequence when rotating due to the reorientation of the light (white, light grey, dark colours), while the voids remain dark grey. The XPL image was subsequently subtracted from the PPL image so that the white and very light grey coloured quartz minerals are not considered as voids. The resulting image was converted into a binary black and white image using the 'threshold' function ('imager' package). The ratio between voids and non-voids was calculated in R environment (R Core Team, 2013). The different types of voids in the samples were analysed by manual micromorphological observations considering each objective lens size at each 1 cm step, classifying voids into seven classes (simple packing voids, complex packing voids, close complex packing voids, channels and vesicles, chambers, vughs and planes) based on the types of relevant voids (Stoops, 2021).

Table 1
Sampling sites. UTM zone (WGS84) for coordinates in Germany: 33U; UTM zone for coordinates in Ethiopia: 37N.

Site	Sample name	Sample description	Easting	Northing
G1 Grunewald Forest Berlin, Germany	Sample G1 footpath (G1F)	Upper 15 cm at the footpath's centre	377310	5814150
	Sample G1 control (G1C)	Upper 15 cm, 1 m off the footpath	377312	5814150
G2 urban park Berlin, Germany	Sample G2 footpath (G2F)	Upper 15 cm at the footpath's centre	387871	5810170
	Sample G2 control (G2C)	Upper 15 cm, 1 m off the footpath	387870	5810172
G3 Ore Mountains, Germany	Sample G3 footpath (G3F)	Upper 15 cm at the footpath's centre	341430	5596508
	Sample G3 control (G3C)	Upper 15 cm, 1 m off the footpath	341429	5596502
Rama depression, Tigray	Sample Rama footpath (sample R)	1.5–8.5 cm below surface at the footpath's centre	479263	1590134
Yeha archaeological site area, Tigray	Sample Yeha footpath (sample Y)	6–19 cm below surface, at the footpath's centre	494455	1574326
	Sample Yeha footpath margin (sample Y*)	3–10 cm below surface, at the footpath's margins	494639	1572953
Hawelti-Melazo archaeological sites area, Tigray	Sample Melazo footpath (sample M)	6–13 cm below surface at the footpath's centre.	478804	1557436

3.4. Sedimentary analysis

The bulk samples were dried at 105° C in a drying cabinet and aggregates were disintegrated using a porcelain mortar. By dry-sieving sample material was subdivided into grain-size classes with diameters >2 mm, ≤2mm and ≤1 mm. The grain-size fraction with diameters ≤1 mm was further measured using a LS 13320 PIDS Beckmann Coulter Laser particle size analyser to obtain the grain size distributions. The ≤1 mm fraction was additionally chemically analysed. The respective sample preparation and measurement steps were conducted according to previously published workflows (Nykamp et al., 2020; Kirsten et al., 2021). Measurement of the electrical conductivity (μS cm^{-1}) and pH values of the water saturated samples was determined in a 1:2.5 solution of air-dried sediment and bi-distilled water using handheld electrical conductivity and pH meters accordingly (Hanna Instruments). Total carbon content (mass-% TC) was determined using a LECO Truspec CHN and an add-on elemental analyser. Total Organic Carbon (mass-% TOC) was measured following $CaCO_3$ dissolution using katalytic oxidation at 680° C and subsequent Non-Dispersive Infra-Red detection using a TOC-L Shimadzu device. Qualitative analyses of mineralogical compounds were examined by X-ray powder diffraction (XRD) analyses using a Rigaku Miniflex 600. Elemental analysis was carried out using the portable energy-dispersive X-ray fluorescence analyser (p-ED-XRF) Thermoscientific Niton XLt3 measuring the sample in plastic cups sealed by a mylar foil (0.4 μm). The prepared sample-cups were measured for 120 s by p-ED-XRF with different filters. Measurements included four known reference standards (RF3, RF25, RF87, RF89) for device error assessment and calibration (Hoelzmann et al., 2017). Preliminary age assessments were conducted on incised footpaths in Tigray using; 1) carbon dating on the footpath sub surfaces (Supplementary Text 2), 2) Optically Stimulated Luminescence (OSL) dating of fan deposits of a gully initiating from one of the footpaths (Supplementary Text 3, Supplementary Figs. 8-9). Extraction of Short-Range Order (SRO) and pedogenic iron oxides was done following Coward et al., (2017) using 1) Sodium dithionite (0.05 M), 2) Ammonium oxalate/oxalic acid 4:3 (0.2 M) and 3) Sodium pyrophosphate (0.1 M). 50 ml of each solvent was shaken in the dark with 0.5 g of homogenized sample material in a tube for 16 h. Subsequently, samples were centrifuged for 150 min at 4400 rpm and filtered through 0.2 mm nylon membrane filters. The extract supernatants were shortly stored in the dark and Fe contents were measured for the filtered extractant solutions applying Inductively Coupled Plasma Mass Spectrometry (ICP-MS) (Coward et al., 2017). Fe

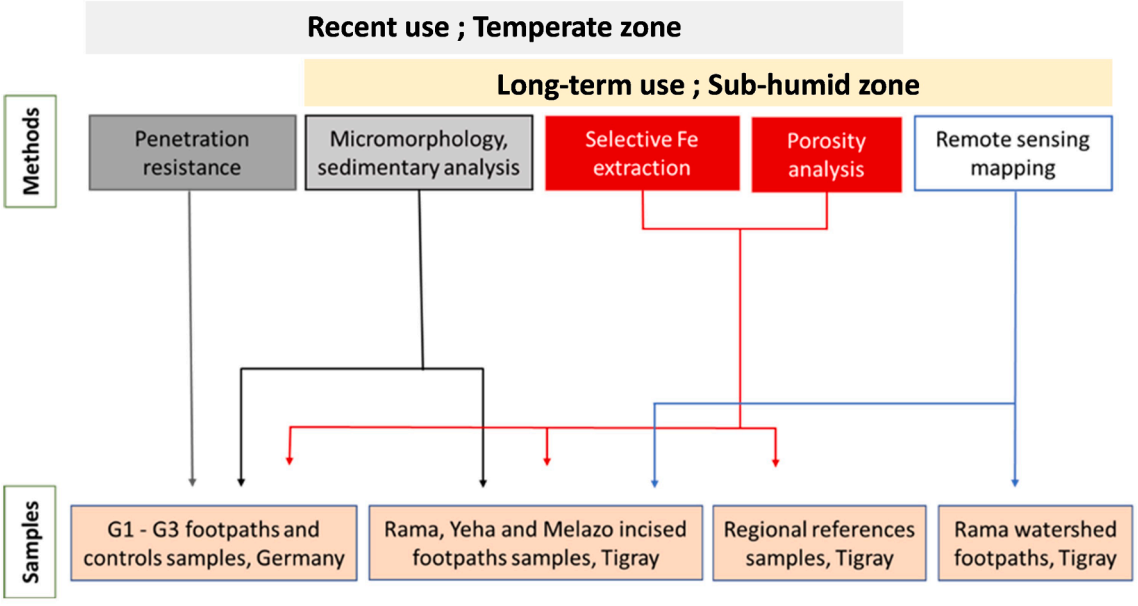

Fig. 5. Flowchart summarizing the various methods and analysed samples. Sedimentary analysis includes grain size analysis, pH, electric conductivity (EC), X-ray fluorescence (XRF) and Total Organic Carbon (TOC). Core analysis including micromorphology, porosity and Fe oxide extraction were performed at all locations. Penetration resistance, which relates to current footpaths surfaces was done for the recently used paths while geomorphological analysis at a watershed scale, looking at long term effects where possible, was done for the long-term used footpaths.

content in soils measured by ICP-MS (ppm) and p-ED-XRF (ppm) has shown high correlation (Kilbride et al., 2006) therefore Fe concentration was normalized and divided by the total Fe concentration evaluated using the XRF. Results for all three extraction methods are given as a ratio between the extracted Fe (Feex) in the footpath sample and the respective Feex from the control or regional reference samples.

3.5. Spatial analysis

In central Tigray, continuous human occupation is expressed by the archaeological records, while geomorphological observations revealed shallow sunken lanes and gullies occupying and accompanying footpaths. Industrialized agriculture and infrastructure are rare, thus in many areas, human-made terraces and footpaths are the main human impact on the landscape. In Germany, in contrast, the intense modern land use and high settlement density did not allow for straightforward mapping of footpaths. Therefore, only in Tigray a spatial analysis was conducted to study possible long-term geomorphological effects resulting from likely historical footpaths. Incised footpaths and streams in Tigray were mapped at a scale of 1:1500 using 1 m/pixel resolution provided by CNES/Airbus Maxar Technologies Map data @2020 as they appeared on Google Maps via the Quick map service extension in QGIS version 3.4.5-Madeira (R Core Team, 2013; Jammalamadaka and Sengupta, 2001; QGIS.org, 2021). The imagery was used to map the three incised Ethiopian footpaths that were sampled (Rama, Yeha and Melazo footpaths) as well as for high resolution mapping of streams and footpaths in the watershed of the Rama footpath. All mapped incised footpaths were validated and distinguished from non-incised footpaths by field surveys in November 2019. The mapping results were compared with CORONA satellite images, produced by US Central Intelligence Agency (KH4B, 1967; DS1102-2106DF072_c) dating to 1967 (USGS) in order to confirm that only footpaths with a minimum age of ca. 50 years were considered in the analyses. The orientations and lengths of non-incised footpaths, incised footpaths and streams were analysed in R environment using circular statistics and rose diagrams, while 'Mean Resultant Lengths' (MRL) was used to indicate the intensity of directionality (R Core Team, 2013; Jammalamadaka and Sengupta, 2001; QGIS.org, 2021).

4. Results

4.1. Macroscopic observations

G1 samples (Grunewald Forest Berlin). In the G1 control sample, the upper 3 cm consist of loose organic material, roots and grasses in particular. These are embedded in sandy humus, while below 3 cm depth a sandy matrix occurs with only occasionally grass roots occurring. The G1 footpath sample had a 5 cm thick upper layer of mixed sands and silts and more diverse and smaller sized organic components than the upper part of the G1 control sample. These top 5 cm are also far more compacted than the upper layer of the G1 control samples (Figs. 6-7, Table 2). Below 5 cm depth a sandy matrix occurs, but different to the G1 control sample it is dominated by leaves and other poorly decomposed organic materials. The profile of the G1 footpath sample is subsequently subdivided into three layers where the topmost layer (0–5 cm depth) is highly compacted, the middle layer (5–15 cm depth) is composed of loose sand with abundance of organic material and an underlying layer (>15 cm depth), which is similar to the middle layer but without large organic remains (Fig. 6).

G2 samples (Urban park Berlin). The G2 samples (G2 footpath and control samples) have similar upper organic and lower sandy sequences as the G1 footpath and control samples. Except for a higher degree of compaction of the G2 footpath sample compared to the G2 control sample (Table 2), and some grasses growing on the G2 control sample's surface, no clear difference between the material characteristics of both samples is macroscopically evident.

G3 samples (Ore Mountains). The G3 control sample shows a clear indication of soil forming processes with undecomposed organic material corresponding to an Oe horizon (0–10 cm depth) followed by an organic humified layer corresponding to an Oa horizon (10–16 cm) (Figs. 5-6). Although components of these two horizons of the G3 control sample were also evident in the G3 footpath sample, clear soil forming indicators were absent in the G3 footpath sample. The G3 footpath sample shows two distinct layers with sharp contact, with dark grey colour dominating the upper 9 cm while stark orange accumulation occupies the underlying layer (9–17 cm depth). In contrast to all other samples, in the G3 footpath sample, the bedrock was reached at a depth of 17 cm (Fig. 7).

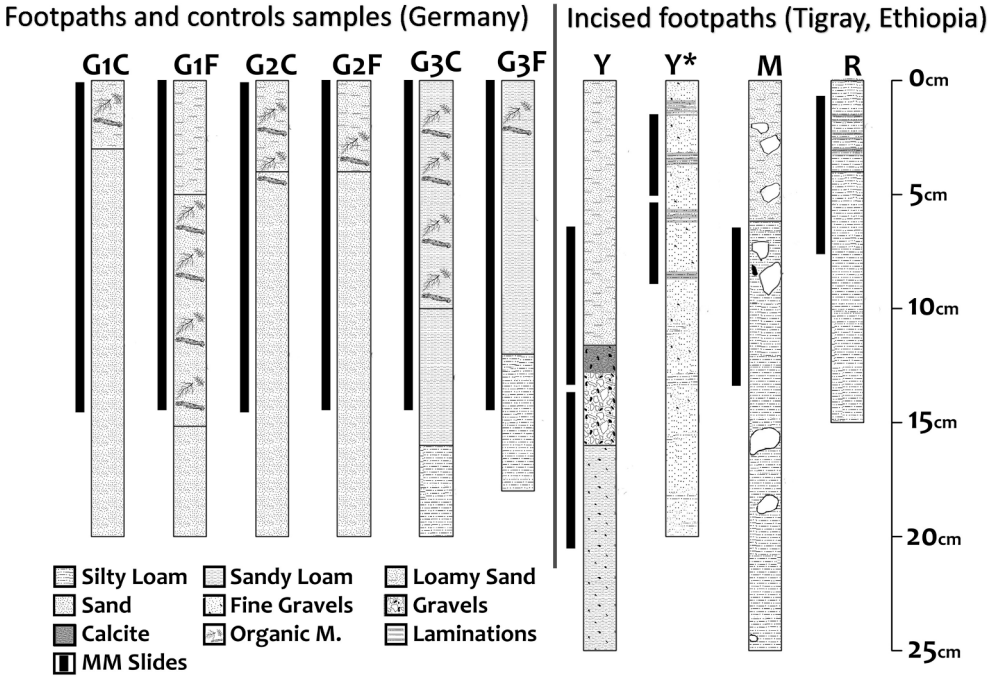

Fig. 6. Section logs of sediment profiles sampled in temperate (Germany; G) and sub-humid (Tigray, Ethiopia; Y, Y*, M, R) climatic zones. Coverage of micromorphological slides (MM) is marked by a black bar. "F" marks samples taken from footpaths, "C" marks non-footpath control samples taken from the undisturbed vicinity of the corresponding footpath sample. (Germany - G1: sampling location in Grunewald Forest, Germany, G2: sampling location at the urban park in Berlin, G3: sampling location in the Ore Mountains, Germany; Tigray, Ethiopia - Y: sampling locations west of the Yeha archaeological site, at the central part of an incised footpath (sample Y) and at the margins of the same incised footpath (sample Y*), M: sampling location at an incised footpath near the Melazo archaeological sites, R: sampling location at a incised footpath in the Rama depression.

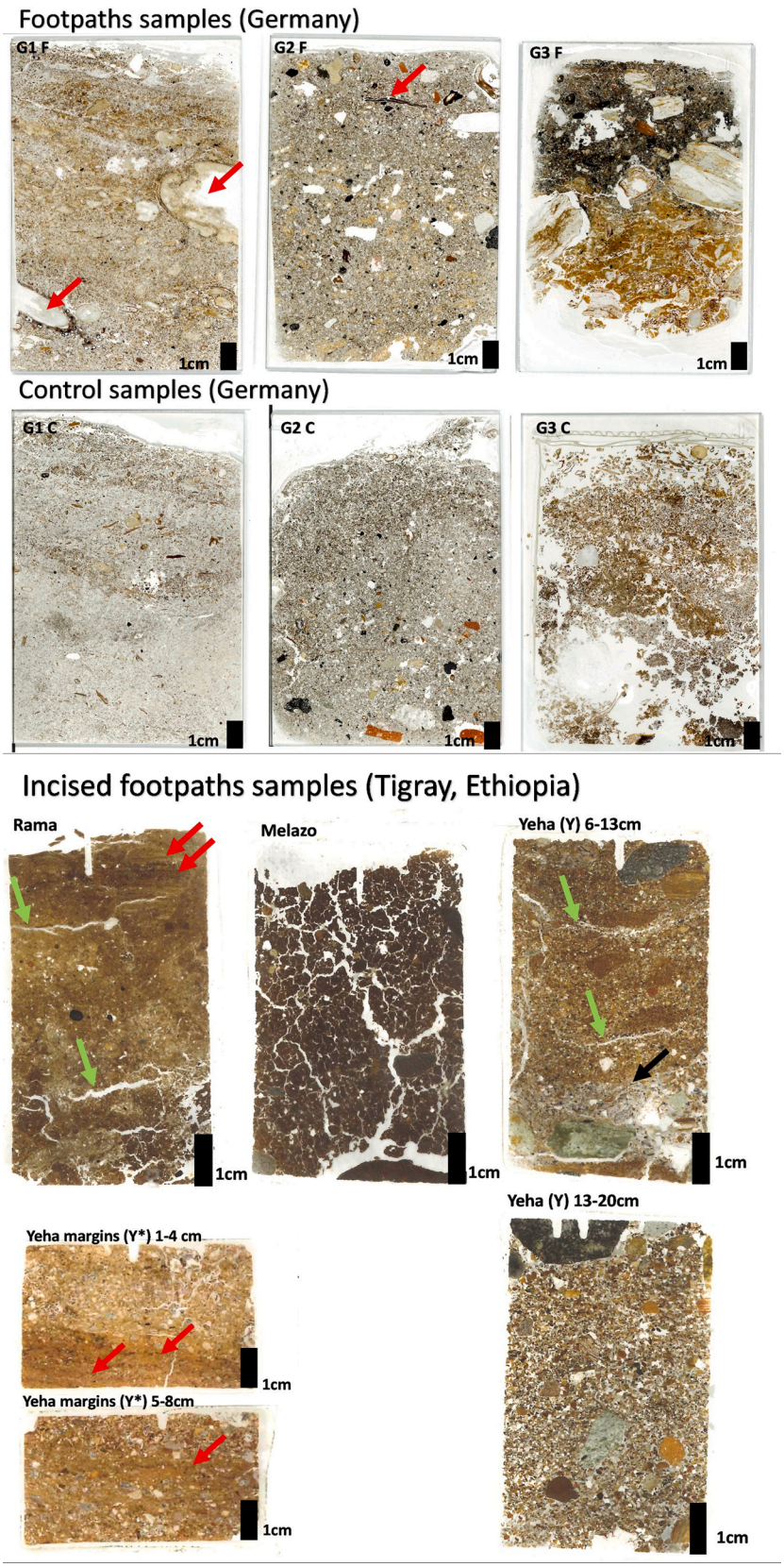

Fig. 7. Upper part: Sampled footpaths from Germany (G1 F, G2 F, G3 F) and their control samples (G1C, G2 C, G3 C). Notice roots in footpath sample G1 (red arrows) and in footpath sample G2 a horizontal thin wooden/charcoal piece that is slightly fractured at its centre (red arrow). Lower part: Samples from incised footpaths from Tigray, Ethiopia (Rama, Melazo, Yeha, Yeha margins,). Notice bedded fine material in both Rama and Yeha margins samples (red arrows) and some horizontal planes in the Rama and Yeha (6–13 cm) samples (green arrow). For the Yeha sample a black arrow points at the contact between the upper fine material and the lower sands and gravel size minerals cemented by calcium carbonate. The latter coarse-grained unit is likely re-deposited and compacted construction material. (For interpretation of the references to colour in this figure legend, the reader is referred to the web version of this article.)

R sample (Rama footpath Tigray). Macroscopically the material of the Rama footpath sample (sample R) showed a homogenous silt-loam texture and did not allow any vertical differentiation.

Y and Y* samples (Yeha footpath Tigray). Sediments extracted from the central part of the main Yeha footpath (sample Y) were silty in the upper part of the subsurface (0–11 cm depth). At the lower part of the subsurface the sediment interchanges between sandy silts and gravels with semi-horizontal orientations (11–25 cm depth). Compared

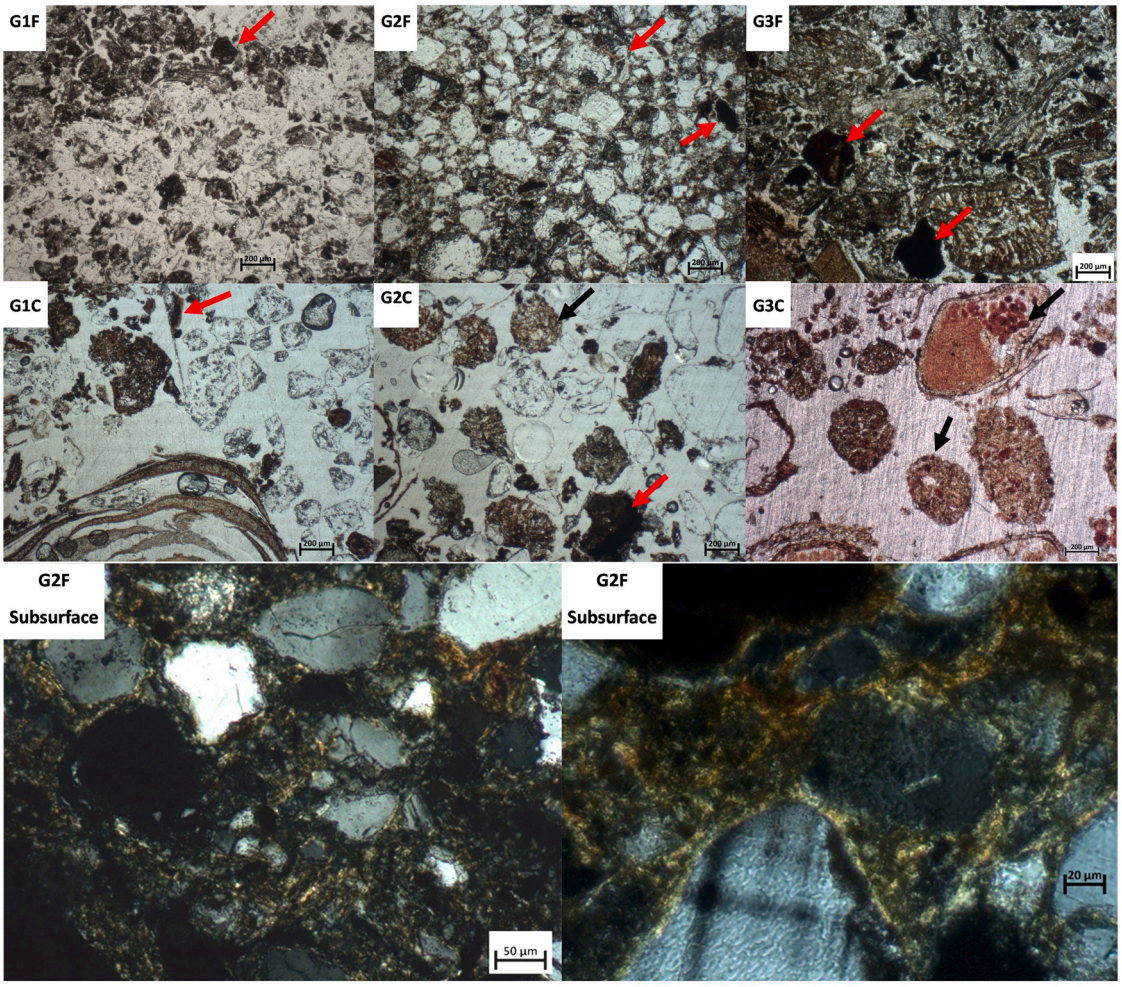

Fig. 8. Surface strata (ca. 0.5 cm below surface) of footpath (F) and control samples (C) of footpaths from the case studies in a temperate zone (Germany; samples G1-G3) in PPL. Microstructures of the three footpaths (samples G1F, G2F and G3F) are massive, while control samples present single grain to crumb and granular microstructures. Notice Fe and Mn nodules and impregnated fine material (red arrows) and organic pellets for the control samples (black arrows). The G2F subsurface images are taken in XPL. Notice the yellow clay particles arranged mostly around grains. (For interpretation of the references to colour in this figure legend, the reader is referred to the web version of this article.)

to the sample Y the sediments of sample Y* originating from a protected location of the footpath were finer and more homogenous (mainly fine sand-silt) excluding only fine gravels (Figs. 6-7).

M sample (Melazo footpath Tigray). In the sample extracted from the Melazo footpath (sample M) heavy clay mixed with low amounts of silts dominated. Occasionally large (3–10 cm long) semi rounded pebbles were embedded into the clayey matrix.

4.2. Micromorphological observations

Micromorphological analysis showed distinctive material differences between the footpaths and structural differences with the control samples (see Supplementary Table 3 for a detailed micromorphological description). Surfaces of all three footpath samples in Germany have massive microstructures as opposed to more granular or crumb microstructures in the surfaces of the control samples (Supplementary Table 3, Fig. 8). The footpath samples G1 (Grunewald Forest Berlin) and G2 (urban park Berlin) show darker and more brown colours compared to the respective more greyish non-footpath control samples (Fig. 7). Additionally, the G2 footpath sample holds a grano-striated (rearrangement of clay particles around grains) and speckled b-fabric causing the brown colour in this footpath (Fig. 8). The brown colour of the G1 footpath sample results from high contents of micro- and macro-organic residues, which are lacking in the more greyish G1 control sample (Supplementary Table 3, Figs. 7-8). Differences between the control and footpath sample, are most striking for context G3 (Fig. 8): While the structure in the G3 control slide shows loose and relatively homogenous composition, the G3 footpath's slide discloses two district strata (0–9 cm depth: dark grey, 9–17 cm depth: yellow-brown) with a clear contact between them. The surface of the G3 control site has an enaulic c/f related distribution with pellets and mesofaunal droppings that are typical of an upper O horizon (Fig. 8). In contrast, the surface of the G3 footpath sample shows a massive microstructure of clayey-silty micromass with an abundance of coarser (medium sand sized) minerals and rock fragments and black-opaque minerals which are black to silver in Oblique Incident Light (OIL), a composition corresponding to the local lithology and possibly affected by modern pollution (Supplementary Table 3, Figs. 7-8).

In the samples originating from the three footpaths sampled in the sub-humid climatic zone (R, Y, M), various forms of massive microstructure and compacted matrixes with partially radiant or semi-horizontal fissure patterns were observed (Figs. 7 and 9). The Rama footpath shows a banded and massive microstructure resulting from layers of clay impregnated with Fe oxide (Fig. 9). The Yeha and Melzao incised footpaths were sampled at a depth of ca. 6 cm below surface in order to recognize possible paleo-surfaces of the footpaths. The sample

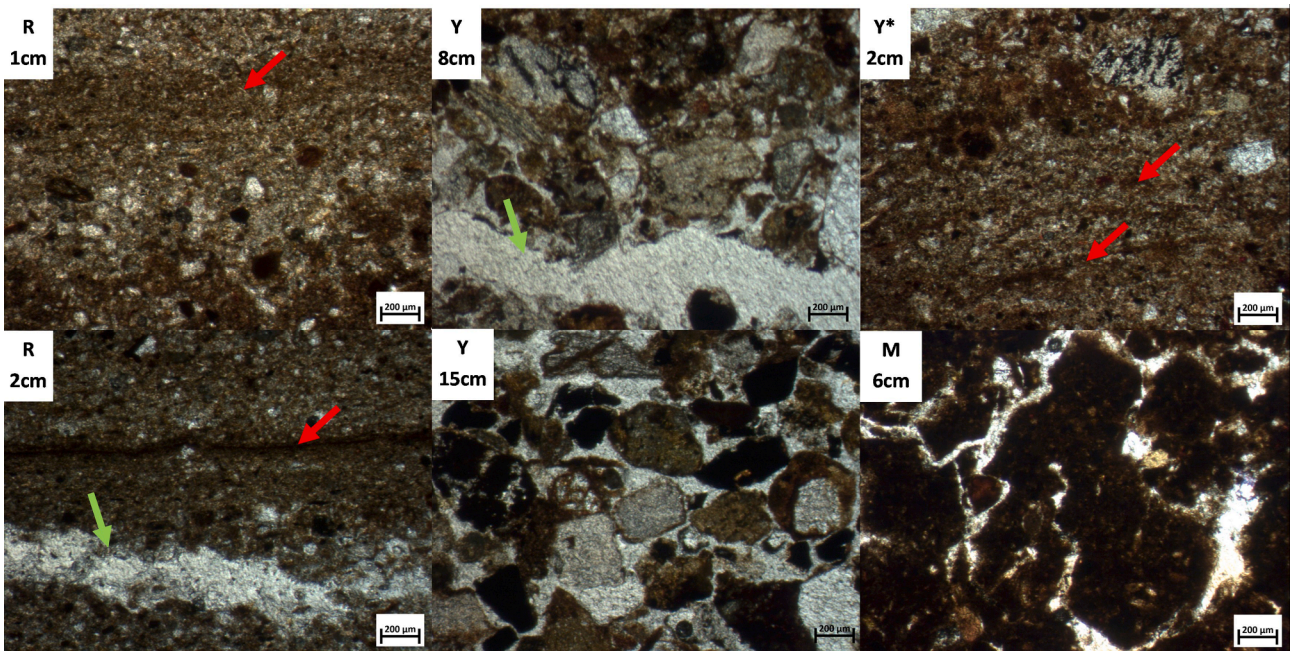

Fig. 9. Different depths below present surface for incised footpath samples from the sub-humid zone case studies (Tigray, Ethiopia). Rama (sample R), Yeha (sample Y), Yeha margins (sample Y*) and Melazo (sample M) incised footpaths. Red arrows point at laminations and bedding suggesting surfaces in the Rama (sample R) and Yeha margins (sample Y*) footpath samples. Green arrows point at horizontal planes found in the Rama (sample R) and Yeha (sample Y) samples. Notice the loose nature of the Y sample at 15 cm below surface as opposed to massive compound upper stratum at 8 cm below surface. Vertical and semi-vertical directions for planes are evident in the Melazo (sample M) footpath sample. (For interpretation of the references to colour in this figure legend, the reader is referred to the web version of this article.)

Table 2
Penetration resistance, pH and electric conductivity for G1-G3 footpath and control samples. Penetration resistance error margins are due to an average of n = 3 at each sampling location using a pocket penetrometer.

Sample	Penetration Resistance kg*cm^{-2}	cm depth below surface	pH	EC µS*cm^{-1}
Sample G1 footpath (G1F)	4.3 ±0. 1	0–3.5	5.1	153
		3.5+	5.4	73
Sample G1 control (G1C)	2 .0 ± 0.2	0–1.5	4.8	150
		1.5+	4.9	56
Sample G2 footpath (G2F)	4.4 ±0.1	0–6	6.8	58
		6+	7.1	73
Sample G2 control (G2C)	2 ±0.4	0–6	6.2	31
		6+	6.6	67
Sample G3 footpath (G3F)	3.5 ±0.5	0–7	4.6	354
		7–13	4.3	310
Sample G3 control (G1C)	0.75 ±0.3	0–8	3.5	378
		8–15	3.4	377

from Yeha footpath centre (sample Y) shows a massive microstructure very heterogeneous in grain size and mineral content and possibly containing redeposited calcitic construction materials (Figs. 7 and 9). The underlying stratum of the Yeha footpath sample Y (12–18 cm below surface) is more homogeneous than the upper stratum, with coarse sands and gravels dominating than the overlying (6–12 cm depth) (Figs. 7 and 9).

4.3. Void analysis

Void frequencies were analysed as a measure for evaluating soil porosity. Differences in porosity between all footpath samples and their respective control samples (samples G1, G2 and G3) or incised footpaths and their regional reference samples (samples R, Y, Y*, M and regional reference samples 1–10) are compiled in Fig. 10. Trends of decreasing relative porosity with increasing depth can be observed for currently used footpaths by analysing the macro voids visible in x2.5 and x5 objective lenses (Fig. 10). For the incised footpaths that were sampled below the current surface (samples Y and M), abrupt changes of macro porosity (x2.5 and x5 objective lenses) are evident. Meso porosity (x10 objective lens) in currently used footpaths (samples G1-G3), and the Rama footpath sample (sample R) is lower than their respective control samples and the regional reference samples for the first 3 cm depth below surface (Fig. 10). Consistent differences in micro porosity (visible in x20 and x40 objective lenses) were not observed. A test was conducted to examine whether there is significantly lower porosity in footpaths from Germany (samples G1F, G2F, G3F) compared with their control samples (samples G1C, G2C, G3C) and for the sample from the (currently used) incised footpath in Tigray (sample R) compared with its regional reference samples (samples 4–8). The T-test considers the entire upper 5 cm of each footpath and control sample (Supplementary Fig. 5). Results show that the sample from the Ore Mountains Forest footpath (sample G3F) has significantly less voids than its control sample (sample G3C) independent from the objective lens sizes while the sample from the Grunewald Forest footpath (sample G1F) has significantly less voids than its control sample (sample G1C) considering the macro and meso voids objective lenses x5 and x10. Differences in porosity between the footpath sample from the urban park (sample G2F) and its control sample (sample G2C) are not significant for the entire 5 cm below surface ($p > 0.5$; Supplementary Fig. 5). The sample from the Rama incised footpath (sample R) from Tigray, shows significantly less voids than two of its regional reference samples (samples 6, 7) applying all objective lens sizes and significantly less voids are visible in the objective lens sizes x2.5, x5, x10, x20 than in the regional reference sample (sample 4). Compared with regional reference sample 5, significantly lower void cover in the sample originating from the Rama footpath (sample R), only occurs for voids visible at objective lens sizes x10 and x20. Compared with regional reference sample 8, footpath sample R has significantly lower micro porosity as visible at objective lens size x20 (Supplementary Fig. 5).

For the samples originating from recreational footpaths located in

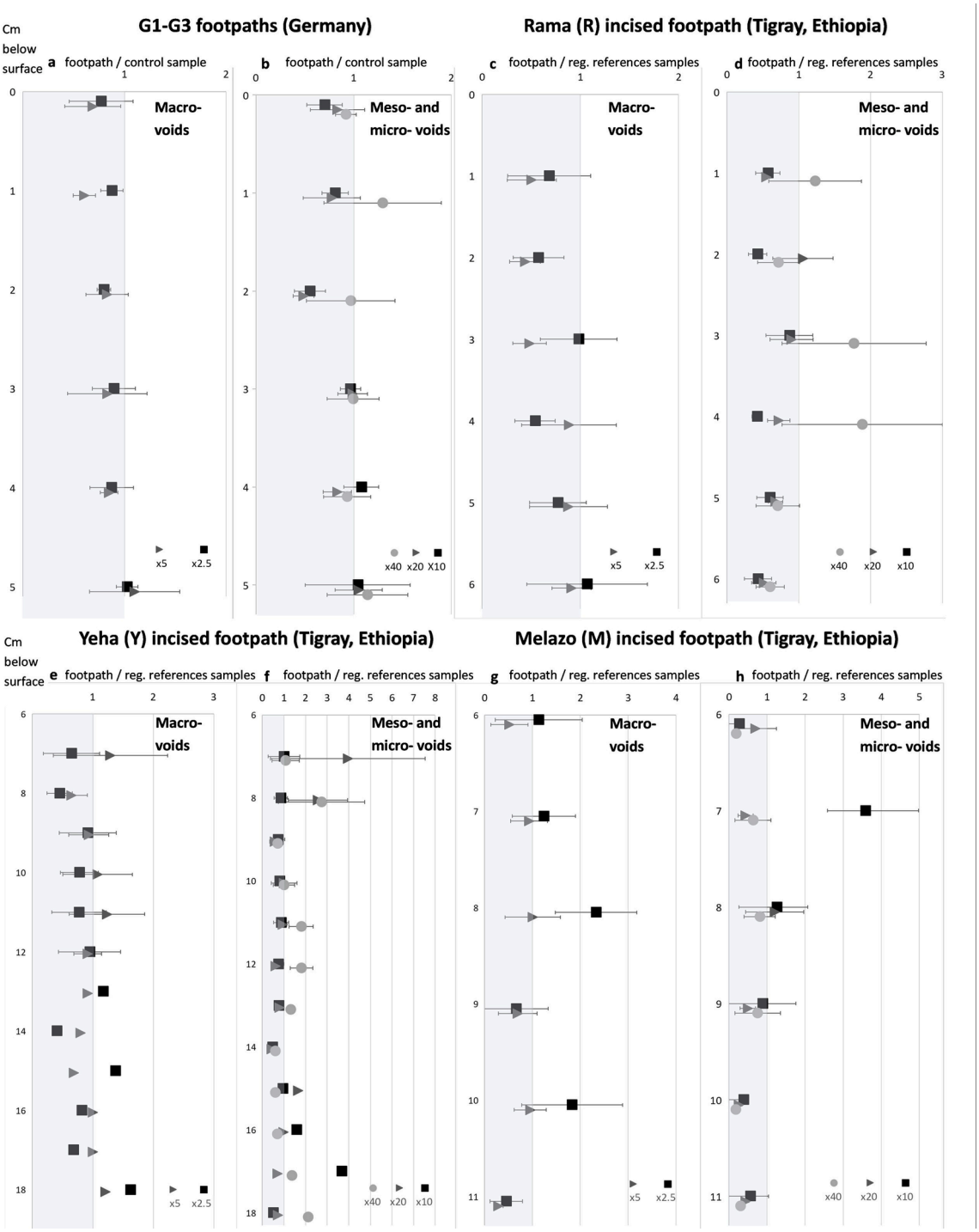

Fig. 10. Relative differences in porosity between samples originating from footpaths, and their respective control samples and regional reference samples (reg. references), as measured using voids frequency difference analysis ('imager' package in R environment). Grey area below 1 indicates footpath has less voids than its non-footpath control sample or regional reference sample. a-d: Comparison between recently used footpath and control samples (n = 3) or regional references in different objective lenses. e-h: Long-term used incised footpath samples (Y and M) in Tigray, Ethiopia compared with regional reference samples in different objective lenses. Regional reference samples: Rama n = 5, Yeha (sample Y) upper slide n = 5, Yeha (sample Y) bottom slide n = 1 (with comparable grain sizes and structure), Melazo n = 7.

the temperate zone, less planes are recognized in the lower objective lens (x5), when compared with their control samples (Supplementary Fig. 6). For the samples originating from the incised footpaths and reference sites in the sub-humid (to semi-arid) zone, an increase in planes and decrease in channels occurs in the samples originating from footpaths compared with the respective regional reference samples (Supplementary Fig. 6). Applying the objective lens (x40), focusing on the smallest recognizable micro voids in samples G1F-G3F, channels appear, while they are far less represented in the respective control samples (samples G1C-G3C). In the samples originating from Tigray (samples R, Y, Y* and M), planes and complex packing voids are more dominant in the samples extracted from incised footpaths compared with those of their regional reference samples (Supplementary Fig. 6).

4.4. Elemental and chemical components

X-Ray Fluorescence (XRF) analyses are presented for the samples from Germany (G1-G3) differentiating between surface and subsurface samples (Table 3). XRF results reveal higher amounts of Pb in the footpath's surface compared with all other samples and that Fe and Al are abundant in all G1 samples (Table 3 and supported by XRD results: Supplementary Fig. 7). The G2 samples have no distinct differences between the footpath (G2F) and control samples (G2C) in XRF data. Fe, Al and Mn are abundant in all G2 samples. For the G3 footpath samples, XRF data shows differences between the G3F sample surface and the G3 control samples with ca. twice as much Fe and three times higher Al contents in the G3F surface sample compared to the respective G3 control samples (Table 3 and supported by XRD results: Supplementary Fig. 7).

4.5. Pedogenic Fe oxides

Pedogenic iron contents (Feex) are higher in the surface samples of all footpaths than Feex contents of their respective control surface samples (Fig. 11a, apart from pyrophosphate for G1). In contrast, Feex contents of subsurface samples in G1-3 were lower in the samples originating from the footpaths than in their control samples (Fig. 11a). Fig. 11b presents Feex values normalized to total Fe concentration measured using XRF (Feex/Fe XRF). Considering the total Fe XRF concentrations, sodium dithionite extracted Feex, that includes most crystalline pedogenic Fe(III) oxides, shows higher contents in all current and reconstructed historical surfaces samples from footpaths than in their controls or respective regional reference samples (Fig. 11b). The oxalic acid extraction method shows a decrease in relative Feex/Fe XRF content with depth in footpaths (samples G1F-G3F) compared with their respective control samples (samples G1C-G3C; Fig. 11b). Oxalic acid extraction accounts for both Short-Range Order (SRO) Fe(III) as well as some pedogenic crystalline Fe(III) oxides.

Table 3
Selected chemical components based on X-Ray Fluorescence (XRF) and Total Organic Carbon (TOC) determination in both strata where direct controls samples where obtainable and comparable (currently used footpaths and their control samples in Germany). For Fe, and TOC obtained from all footpath samples see Supplementary Table 5.

Sample		Fe ppm	Al ppm	Mn ppm	Pb ppm	P ppm	TOC mg/L
G1C	Surface	4062 ± 52	9435 ±476	<d.l.	<d.l.	<d.l.	177
	Subsurface	3555 ± 50	10,011 ±526	<d.l.	<d.l.	<d.l.	75
G1F	Surface	4746 ± 59	8138 ±500	<d.l.	13 ±2.2	<d.l.	214
	Subsurface	5252 ± 68	10,816 ±638	<d.l.	<d.l	<d.l.	147
G2C	Surface	13,493 ± 104	20,614 ±671	<d.l.	79 ±4	<d.l.	72
	Subsurface	7631 ± 100	15,657 ±1001	173 ±39	<d.l.	<d.l.	215
G2F	Surface	14,365 ± 107	23,747 ±717	<d.l.	110 ±4	<d.l.	61
	Subsurface	16,733 ± 116	25,961 ±697	55 ± 28	29 ±3	<d.l.	40
G3C	Surface	36,804 ± 243	20,903 ±1078	130 ±36	99 ± 4.8	1953 ±118	988
	Subsurface	51,648 ± 247	52,276 ±1156	<d.l.	213 ± 5.54	419 ± 73	654
G3F	Surface	101,603 ±434	78,418 ±1581	555 ±37	98 ± 4.85	596 ± 69	355
	Subsurface	67,029 ± 313	83,804 ±1653	398 ±35	72 ± 3.97	318 ± 71	247

Error margins - XRF device error per sample. < d.l – Values for element are lower than the device's detection limit.

4.6. Antiquity and spatial analysis

In Tigray, non-industrialized land use and cover enables the spatial analysis of the studied incised footpaths (Rama, Yeha and Melazo footpaths). The latter were subsequently mapped and spatially characterized on a watershed scale (Supplementary Table 6). Identifying these footpaths on basis of CORONA satellite images from 1967 (USGS) reveals that the historically used incised footpaths in Tigray already existed to various extents at least 50 years ago; however, the degree of incision remains unclear due to image resolution. For the Yeha footpath (sample Y), it seems that the agricultural area around the footpath had decreased dramatically along with the construction of the nearby road which was also built on top of parts of the older footpath. While accurate dating of footpaths use is challenging, preliminary dating attempts were conducted using two separate proxies. Dating sediments directly under footpath surfaces using ^{14}C, can indicate either pedoginic carbon formation or burial and subsequently the latest possible time of accumulation or soil formation. The ages of the dated soil carbon from ca. 20 and 5 cm below the surface of the Yeha incised footpaths (Y), are 1285 and 215 years BP accordingly. The ^{14}C sampling locations exhibited footpath related features (see micromorphology), suggesting these dates account for the use of the surface as a footpath. Using ^{14}C results in this context can only serve as supportive circumstantial evidence for the likely antiquity of footpaths, as older ^{14}C bearing organic matter could have been eroded and redeposited. Separately, fan deposits of a gully initiating from a footpath in the Rama watershed was dated using luminescence dating (Supplementary text 3). The latter is assumed to indirectly date the establishment of the footpath, as the erosion resulted from the surface runoff generated from the footpath. Using a luminescence dating approach for the dating of single grains of potassium-rich feldspar, which has proven to be suitable for the dating of sediments prone to incomplete bleaching (García et al., 2021), the fan deposits were successfully dated to 1.5 ± 0.2 ka (see Supplementary Text 3 and Supplementary Figs. 8-9 for details). This indirect age estimate is in general agreement with the lower end of the age range obtained from radiocarbon dating and provides additional evidence for the antiquity of the footpaths in Tigray (Supplementary Texts 2–3).

In the Rama drainage basin (Fig. 12), orientations of incised footpaths show clear and distinct similarities to the orientation of the stream network as opposed to the unoriented non-incised footpaths (Fig. 13). Additionally, 57 gullies have initiated ('gully heads') in the 5 m away from non-incised footpaths while only 5 gully heads were found within the same distance from incised footpaths. Normalizing these values using the lengths of footpaths, indicates that the amount of gully heads per 100 m of non-incised footpaths are one order of magnitude higher than that of gullies initiating next to incised footpaths (Supplementary Table 7).

5. Discussion

5.1. Structural patterns

Footpaths located in different climatic zones and under different land uses, hinder or promote natural surface processes distinctively and to various extents. However, from their comparison, some common patterns do emerge. Similar to the effect of heavy machinery usage in forests as well as pressure caused by farming vehicles (Bagheri et al., 2012; Batey, 2009; Silva et al., 2011), footpaths show a tendency for lower porosity compared to the control samples in both sub-humid and temperate climate zones (Fig. 10, Supplementary Fig. 5). Micromorphology confirms a similar observation made on compaction by humans or animals, which affects the soil and vegetation of footpaths at similar depths (Yaşar Korkanç, 2014; Tejedo et al., 2016; Sherman et al., 2019; Roovers et al., 2004). Trampling and soil formation appears to be one of the main processes influencing macro- and micro differences in the temperate environment, while the interaction between trampling and

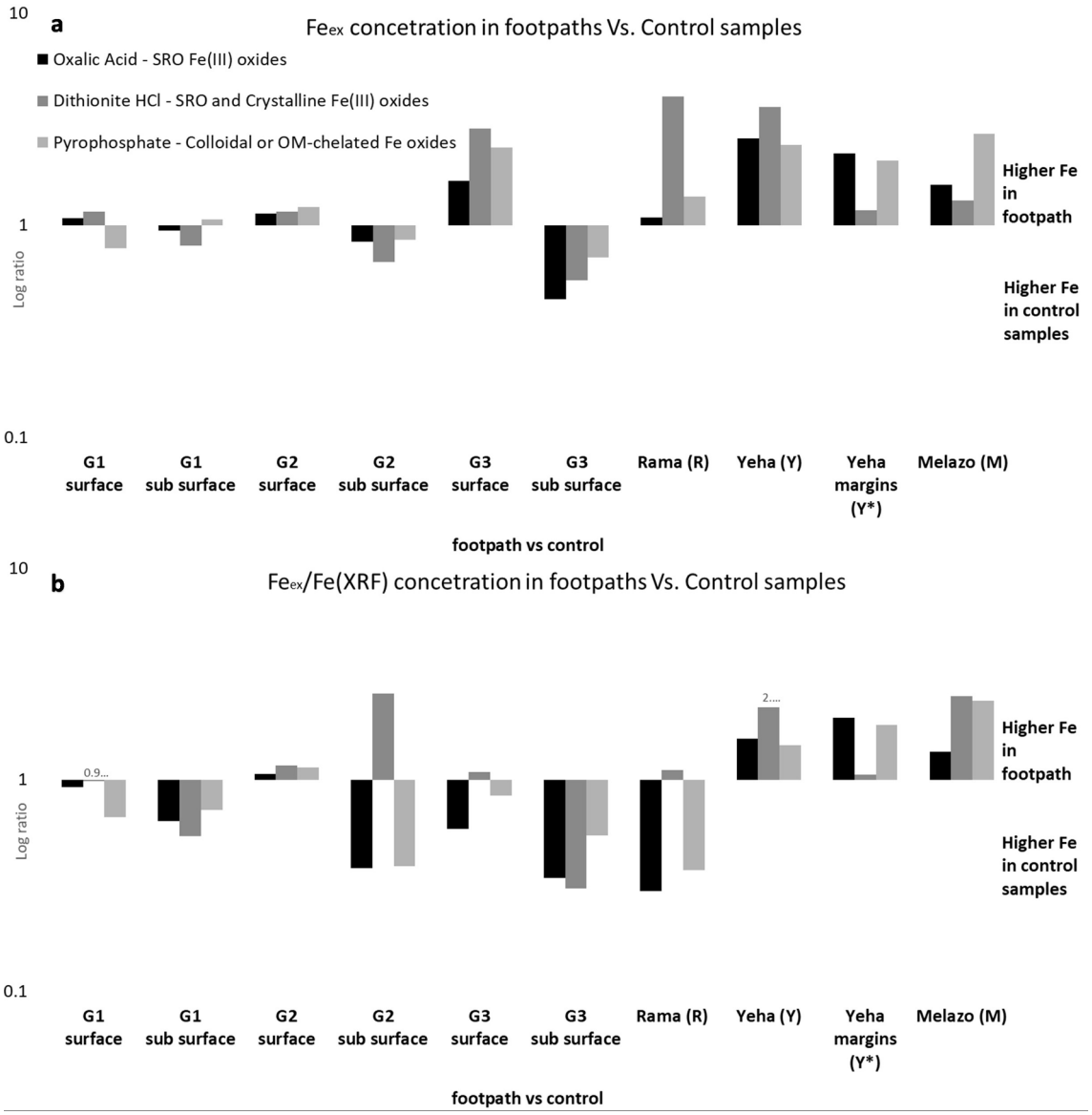

Fig. 11. Three types of Fe extraction (Feex); Oxalic Acid (black), Sodium Dithionite HCl (dark grey) and Sodium Pyrophosphate (light grey). For G1-G3 Feex from currently used footpaths, Feex is divided by their control samples for the surface (ca. 0–7 cm) and subsurface (ca. 7–15 cm) of each location. For the incised footpath samples, Rama (sample R), Yeha (sample Y), Yeha margins (sample Y*) and Melazo (sample M), Fe was extracted at 1–8, 2–5, 6–12 and 6–15 cm below surface accordingly. The Feex values were divided by Feex values extracted from the subsurface of the closest and most similar in grain size regional reference sample (regional reference 9 for R, 11 for both samples Y and Y* and at the location of reference 6 for sample M). All values are in logarithmic ratio. Fig. a. shows Feex values and b. Shows Feex values normalized to total Fe, obtained using X-Ray Fluorescence; Feex/Fe (XRF).

sedimentation-erosion is dominant in the sub-humid Tigray region. This difference can have great impact on a possible positive or negative effect of footpaths on the topsoil. Footpaths from the sandy soils in the temperate zone (GF1-2) are more compacted, with finer grains and have a more massive microstructure than their control samples (Figs. 7-8). Similarly, there is a massive microstructure evident in the upper stratum of the likely historical sunken lane Yeha (footpath sample Y, Figs. 7-9). Although channels and Fe oxides (indication of pedogenesis) are evident, much of the contacts between units and features in the Y footpath sample indicate that the groundmass organisation is more a result of compaction than bioturbation (Fig. 9). Additionally, the underlying stratum sedimentary deposition in Yeha suggests that medium energy running water was responsible for the deposition of the earlier phase of the Yeha footpath (sample Y) sediments (Leopold et al., 2020). The Rama footpath (sample R) shows similarities (Figs. 7 and 9) to footpaths in lake marl sediments, where trampling initiated the formation of a flat depression and was subsequently filled with laminated puddles and fine sediments (Rentzel et al., 2017). Generally, the banded and massive microstructure with fine layers of clay impregnated with Fe oxide in the R footpath in the sub-humid zone (Fig. 8), is likely an indication of a buried surface horizon (Verrecchia, 2021; Rentzel et al., 2017). Grain size seems to play an important role in both climatic zones, as the pattern of lower porosity in footpaths compared to the control samples is unclear for the clay rich sample in the sub-humid zone while the other samples show similarities to the temperate zone footpaths (Fig. 10). One explanation is that smectite undergoes seasonal shrink and swell cycles that have shown to affect soil porosity (Rasa et al., 2012; Pires et al., 2009). Such cycles may have impeded the preservation of a possible imprint resulting from the footpath formation. However, micromorphological experimental work by Bresson and Zambaux (1990), imitating heavy machinery pressure, showed three main factors influencing the intensity of fissures; (1) the degree of

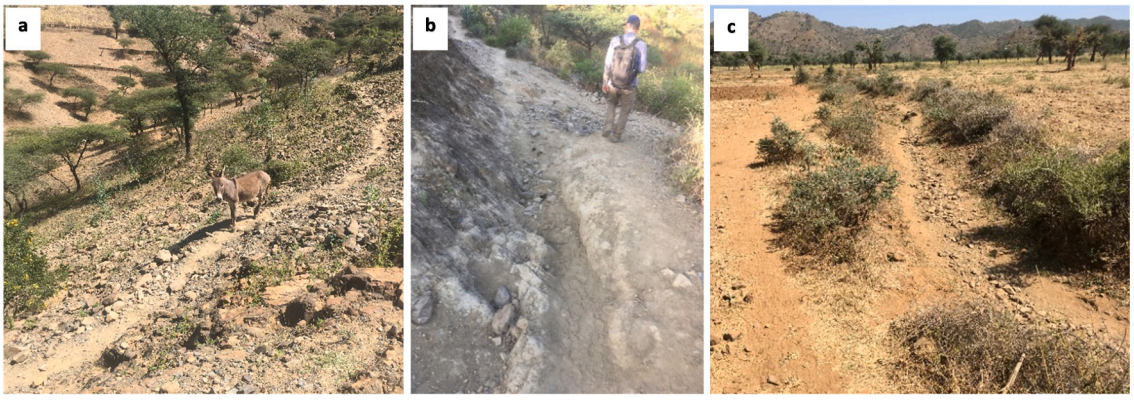

Fig. 12. Field photographs from the Rama drainage basin: a. a typical non-incised footpath, b. an incised footpath (shallow sunken lane), c. a segment of the sampled Rama incised footpath.

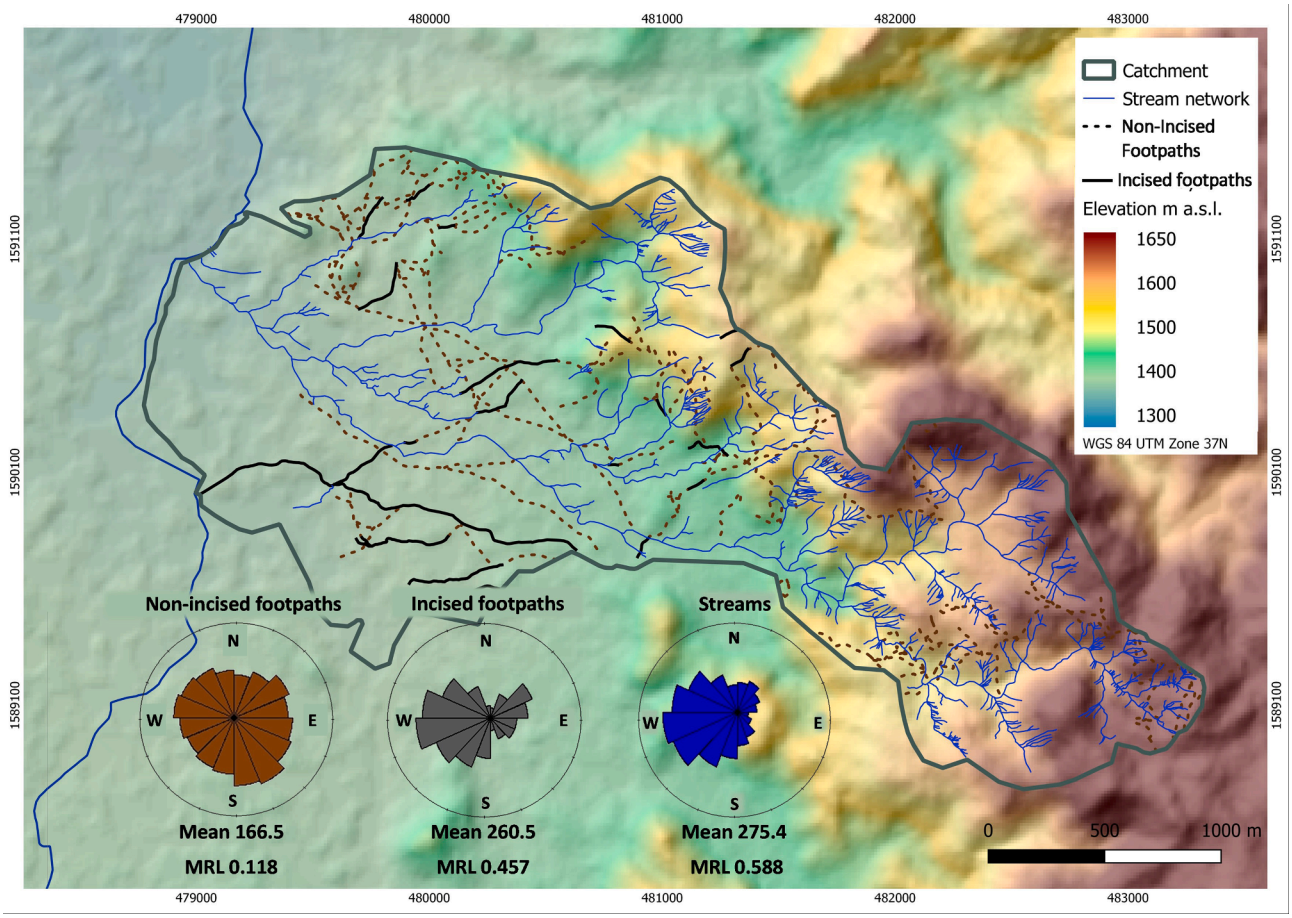

Fig. 13. The Rama watershed case study. Rose diagrams indicating directions of non-incised footpaths, incised footpaths and streams. Mean averaged direction was calculated for each feature. Mean Resultant Lengths (MRL) indicates the intensity of directionality, with 0 representing no preferred orientation and 1 a unidirectional model (Agostinelli and Lund, 2013).

applied pressure, (2) water content, and (3) gravel content and heterogeneity. It was found that higher applied pressure and higher water content generated more fissures. The most distinct case of fissures in our study was observed for the R footpath sample, which receives overbank flow on a weekly basis from the surrounding field irrigation system. Bresson and Zambaux (1990) further concluded that the occurrence of gravels, or a non-homogenous soil matrix, may redirect the pressure, resulting in less fissures. For the M footpath sample, the fine homogenous sediments with few pebbles under the footpath resulted in many fissures and a dense packing, while for footpath samples from the temperate zone (samples G1-G3), which are of coarser grain size, we observed the least amount of fissures. Both findings are in good agreement with the aforementioned experimental work (Bresson and Zambaux, 1990).

5.2. *Void types*

Unlike the larger voids, smaller void types in footpaths do not show a

clear decrease compared with control samples (Fig. 10). From a soil mechanic perspective, the smaller voids may be protected by larger grains and aggregates from pressure applied to the surface, hindering the effect of compaction on porosity. If water supply is a factor responsible for the decrease in porosity under footpath samples, it has been observed that during wet-dry cycles the larger voids are those mainly experiencing enlargement. In the case of footpaths, lack of such cycles under the footpath, while they occur in control samples, may present the opposing side of a similar process (Pires et al., 2009). Looking into the type of voids, it should be stated that images gained in 1 cm steps to classify void types as conducted here (Supplementary Fig. 6), could produce slightly different results compared with a manual qualitative assessment of void types along a slide (Supplementary Table 3). Furthermore, both types of observations are limited in producing a representative database as a micromorphological slide captures only several cm in depth and incorporates a two-dimensional view (Stoops, 2021). In the temperate climate zone, footpaths have higher relative number of vughs than their control samples where planar voids occupy more of the relative space (Supplementary Fig. 6). This difference could be a direct result of compaction, by which elongated voids, such as planes or channels, are destroyed and more disconnected patterns, such as vughs, occur (Nicosia and Stoops 2017; Stoops 2021; Rentzel et al., 2017). Differently appearing but perhaps a result of a similar process, in sub-humid footpaths, planes are more abundant in the footpaths compared with the regional reference samples. This effect is mostly at the expense of channels, which are more abundant in the reference samples (Supplementary Fig. 6). Although the two patterns may seem contrary, the footpath-related compaction in the finer and drier sediments of Tigray, could have altered the more rounded channels to form the rather angular planes, in accordance with the effect of compaction of finer grain sizes (Bresson and Zambaux 1990). However, the formation of channels, that are largely related to bioturbation, is also dependent on the availability of water and the infiltration capacity (Pietola et al., 2005; Sherman et al., 2019; Jim 1993; Ayres et al., 2008). This is in agreement with results of Shipitalo et al. (2004) who observed for finer grain sizes that larger voids result from the works of burrows, earthworms and cracking (Shipitalo et al., 2004). Therefore, a lower number of larger planar and channel voids (Supplementary Fig. 6) could also be due to a decreasing effect of bio- and pedo-features, rather than strictly from direct surface pressure (trampling). The latter process supports an interpretation as for the hindering of soil formation in footpaths under temperate climate. The other agent likely having the strongest effect on the formation of larger voids are large surface roots. Reduction of surface vegetation on footpaths reduces roots, increases the bulk density and reduces water permeability (Sherman et al., 2019; Ayres et al., 2008; Cole, 2004).

5.3. Pedogenesis

In all currently used footpaths (in Germany and Tigray), there is little indication of soil formation/bioturbation in the upper 3 cm (apart from the few mentioned pedogenic Fe oxides in Tigray, Figs. 7 and 9). In the Ore mountains (G3), the control sample shows enaulic c/f related distribution with pellets, mesofaunal droppings and higher organic carbon (Fig. 8, Table 3) that are typical of an upper O horizon, which are absent in the footpath (Verrecchia, 2021). In the latter footpath sample (G3F), both structure and organic materials in the subsurface stratum have likely developed prior to the surface being compacted and used as a footpath. This stratum has an erosional contact to the surface layer, suggesting the missing O horizon may have been eroded along the footpath. In the temperate zone sandy footpaths (Berlin), the darker colours (in visible light, Fig. 7) as opposed to light grey in their respective control samples, has to do both with higher clay (G2) and organic matter (G1) contents in the footpaths. The higher clay content is likely resulting from direct pressure rearmament (Fig. 8). Organic matter is stabilized by trampling as reduced pore volume impedes microbial activity (Silva et al., 2011; Guimarães et al., 2013; Mikutta et al., 2006). Neve and Hoffmann (2000) showed that the carbon mineralization rate decreases with specific bulk densities, indicating that carbon mineralization in compacted soils can lead to an increase in the accumulation of organic matter (Neve and Hofman, 2000). Therefore, by decreasing air and water supply, trampling hinders the degradation, humification and mineralization of organic matter. Following this, it appears that in the sandy soils, footpaths preserve organic material due to hindering of air and water supply while still receiving leafs and organic deposits from nearby sources. In silty-clayey soils of both climatic zones, an opposite outcome emerges, with less organic material than in the control samples, due to erosion and removal of vegetation. Another aspect found in the temperate zone sandy footpaths, is the higher Pb concentration in footpaths than in controls which is likely related to modern traffic pollution (Bartkowiak et al., 2017) and its accumulation may be favoured on footpath surfaces due to compaction as well as lower biogenic activity compared to the control sites (Table 3). Pedogenic iron oxides relate to the amount of oxygen, SOM and water availability affected by soil porosity (Chen et al., 2020; Coward et al., 2017). Compaction and the resultant impeded oxygen supply could be behind the higher Feex content in footpaths surfaces compared with their control samples in both temperate and sub-humid climate zones. Chen et al., (2020) demonstrated how Fe(II) under anoxic conditions generates SRO Fe(III) oxides (Chen et al., 2020). Independently, pedogenic metal oxides have been long known to strongly relate to anoxic and reducing conditions and therefore to changes due to water and air conductivity and supply (Bigham et al., 2002). Independently, changes in Fe oxides have shown to be a direct result of compaction (Coulon and Bruand, 1989). Likely historical footpaths have higher amounts of SRO and poorly-crystalline Fe(III) oxides than their closest regional reference samples of similar depth (Fig. 11). This is in contrast to sub-surfaces of the modern footpaths from the temperate zone, suggesting that the former were in fact past surfaces of the footpaths. Using the XRF normalization on ammonium oxalate Feex extraction, a pattern of higher relative Feex in footpath surface samples compared with their sub-surfaces emerges. The latter may imply a reducing zone of water stagnation on the surface and lack of water supply in the subsurface. In machinery compacted forest soils, citrate bicarbonate extracted Fe is higher in compacted soils than in non-compacted control samples for ca. the upper 30 cm (Nawaz et al., 2016). The authors argue that due to compaction, water resides longer on the compacted surface, reducing the availability of oxygen and changing the Fe lability through reduction from Fe(III) + to Fe(II) + i.e., from well crystallised to poorly crystalized Fe oxides (Nawaz et al., 2016). Similar to an observation made in an experimental trampling site (Rentzel et al., 2017). In the current work, another explanation is possible beyond the *in-situ* pedogenic process. The most consistent Feex increase in the temperate climate zone footpaths' surfaces, following normalisation using XRF, is for the well crystalized Fe(III), suggesting more than just pedogenic origins for the Fe or slow crystallization. Therefore, these well crystalized Fe oxides could have actually been transported and trampled into the footpaths' surfaces by humans and animals rather than being illuviated or bioturbated to the sub surface in the control samples. However, apart from the G3 footpath, there is no indication for such Fe import in the micromorphological samples.

5.4. Long-term used footpaths and linear soil erosion

Unlike the temperate and industrialized central Europe, in the Tigray region, mechanized agriculture, modern infrastructure and urban settlements, have not significantly impacted much of the local landscape. It has been previously shown for the Ethiopian Highlands and elsewhere, that both, pathways and roads, promote the formation of gullies downslope and the formation of sunken lanes due to incision (Nir et al., 2021; Busch et al., 2021; Nyssen et al., 2002; Sidle et al., 2019), as compacted and thus less permeable surfaces result in increased surface

runoff (Boardman, 2013; Sidle et al., 2004; Ziegler et al., 2000; Zgłobicki et al., 2021). The onset of incision along a footpath is likely to initiate only in one (or several) specific location along the path, comparable to trigger factors of gullies, where slope and catchment area thresholds are crossed (Belachew, 2020). In this sense, it differs from a gully as several locations and thresholds can initiate different types of soil erosion in one path, e.g., gullies and sunken lanes. Sunken lanes can play an important role in a catchment's drainage system (Zgłobicki et al., 2021). It is therefore not surprising that within the Rama watershed case study, incised footpaths follow similar general directions as the stream network (Fig. 13). It has been recently shown that unpaved roads may develop different rill structures, depending on the road slope angle (Cao et al., 2021). This mechanism may also govern the incision of footpaths (Fig. 12). It is evident that less gullies tend to form in the vicinity of incised footpaths than near non-incised footpaths (Supplementary Table 6). Changes in surface runoff patterns could be responsible for this observation. When a footpath is parallel to the stream network direction, at least for some of its course, incision along the footpath may occur due to surface runoff either during one or multiple events (Zgłobicki et al., 2021). This type of erosion is depending on the slope angle, suggested to initiate at ca. 7% (Cao et al., 2021). Incised footpaths would subsequently canalize the surface runoff downslope along the footpath. However, in cases where the footpath is not incised, likely when it is perpendicular to the slope, surface runoff due to the footpath's lower permeability (Figs. 7-10), would continue directly downslope from the footpath. Such runoff can initiate gully erosion. These gullies would be perpendicular to the footpath downslope. Due to their compaction and resulting different morphology, it is likely that most incised footpaths, similar to shallow sunken lanes (<0.5 m deep), tend to incise slower than gullies in a similar environment (Zgłobicki et al., 2021). Additionally, it has been observed that incised footpaths in the Rama watershed do not have banks steep enough to collapse (Fig. 12). As a result, in the study area, gullies are usually deeper than incised footpaths. Subsequently, soil erosion and sediment supply resulting from these gullies should be higher than that resulting from incised footpaths. The latter observation, coupled with compositional and micromorphological differences between footpaths and non-footpaths (Figs. 7-10), suggests that footpaths could be considered as Small Natural Features (SNF) that hold the potential to increase local biodiversity (Zgłobicki et al., 2021).

6. Conclusions

The long-term residues of footpaths were evaluated, using tools of different scales in a variety of climatic, sedimentary and land-use contexts. Comparing recreational footpaths in a temperate industrialized European environment with that of the sub-humid, extensive agricultural region of the Ethiopian Highlands, have allowed to observe several common trends. Trampling decreases the porosity of the top 3 cm of the soil while the type of voids under the footpath are more angular than outside the path. Footpaths result in the reduction of biogenic activities due to hindering of oxygen and water supply from the surface. Most extractable pedogenic Fe values are consistently higher on footpaths surfaces than in non-path control samples, likely due to surface processes (e.g. puddles, overland flow, Fe transport) or the result of the lower pedogenesis on the footpath. Differences between the various climatic and sedimentary environments are striking; In temperate environments, footpath formation can erode or hinder soil formation while specifically in sandy forest environments it can also result in burial of organic matter (e.g., leaves), hindering organic decomposition and carbon discharge. Trampling results in higher overland flow and erosion dynamics in all environments with the intensity of these processes depending mainly on the topographic position of the footpath. However, in a sub-humid zone, footpath-erosion interaction seems more dominant and possible to systematically observe. At the latter environment, incised footpaths follow the direction of the stream network and hinder gully erosion downslope from paths. The incision of footpaths rather than the development of gullies, may result in lower soil erosion on a watershed level. Long-term used incised footpaths can be recognized using micromorphology as they are dominated by the interaction between erosion and compaction, while recreational footpaths in a temperate climate zone can hinder soil formation and may also result in lower decomposition of organic matter under the footpath. These preliminary results call for future research into the behaviour of footpaths under different environmental conditions. Such investigations may hold implications for the recognition of older footpaths in archaeological contexts as well as recommendations for organic carbon storage and pathway management to prevent soil loss on a watershed scale.

Declaration of Competing Interest

The authors declare the following financial interests/personal relationships which may be considered as potential competing interests: Nadav Nir reports financial support was provided by Studienstiftung des deutschen Volkes. Brigitta Schuett reports financial support was provided by DFG.

Acknowledgments

In memory of Prof. Georges Stoops. We would like to thank the Authority for Research and Conservation of Cultural Heritage (የቅርስ ባለስልጣን ተወካይ) of the Federal Democratic Republic of Ethiopia: Haileyesus Desta Ayalew, Tsegazeab Mezgebe and Haftum Birhane. We would like to express our deep sympathy for our partners in Tigray in hopes for a sustainable resolution to the current conflict. We would like to thank Christopher Eichhornchen (GIZ) for valuable fieldwork assistance and Peter Schad for his helpful advice. Field work in Ethiopia was conducted as part of the DFG funded project "Routes of Interactions" (Schu949/16; project no. 404354728). Continuous support at Freie Universität Berlin was given by: Fabian Kirsten, Manuela Abendroth, Ralf Milke, Silvan Schmieg and Fabian Becker. We additionally value the assistance of Kristina Pfeiffer (DAI) and Julius Schröder. We would like to thank the editor and the anonymous reviewers for significantly improving an earlier version of this manuscript.

Appendix A. Supplementary data

Supplementary data to this article can be found online at https://doi.org/10.1016/j.catena.2022.106312.

References

Addisie, M., Langendoen, E., Aynalem, D., Ayele, G., Tilahun, S., Schmitter, P., Mekuria, W., Moges, M., Steenhuis, T., 2018. Assessment of practices for controlling shallow valley-bottom gullies in the sub-humid Ethiopian highlands. Water 10 (4), 389.

Agostinelli, Claudio; Lund, Ulric, 2013. R package 'circular': Circular Statistics (version 0.4-7). In URL https://r-forge. r-project. org/projects/circular.

Asfaha, T., Nyssen, J., Negash, E., Meaza, H., Tesfamariam, Z., Belachew, B., et al., 2021. Status of cropping in the wider surroundings of Mekelle. Tigray, Ethiopia.

Asmi, A.N., Othman, N., Zain, M.Z.M., Wahid, M.A., 2020. A Study on Human Foot Pressure Behaviour and Balancing Characteristics. IOP Conference Series: Materials Science and Engineering 884 (1), 012001.

Ayres, EDWARD, Nkem, J.N., Wall, D.H., Adams, B.J., Barrett, J.E., Broos, E.J., Parsons, A.N., Powers, L.E., Simmons, B.L., Virginia, R.A., 2008. Effects of human trampling on populations of soil fauna in the McMurdo Dry Valleys, Antarctica. Conservation Biol.: J. Soc. Conserv. Biol. 22 (6), 1544–1551.

Bagheri, I., Kalhori, S.B., Akef, M., Khormali, F., 2012. Effect of Compaction on Physical and Micromorphological Properties of Forest Soils. AJPS 03 (01), 159–163.

Bartkowiak, A., Lemanowicz, J., Breza-Boruta, B., 2017. Evaluation of the content of Zn, Cu, Ni and Pb as well as the enzymatic activity of forest soils exposed to the effect of road traffic pollution. Environ. Sci. Pollut. Res. 24 (30), 23893–23902.

Batey, T., 2009. Soil compaction and soil management–a review. Soil Use Manag. 25 (4), 335–345.

Belachew, P.H.D., 2020. Hydrological Processes and Control of Gully Erosion in a Watershed in the Sub Humid Highlands of Ethiopia.

Bell, M., Leary, J., 2020. Pathways to past ways: a positive approach to routeways and mobility. Antiquity 94 (377), 1349–1359.

Berhane, A., Hadgu, G., Worku, W., Abrha, B., 2020. Trends in extreme temperature and rainfall indices in the semi-arid areas of Western Tigray, Ethiopia. Environmental Systems Research 9 (1), 1–20.
Bernhardt-Römermann, M., Gray, A., Vanbergen, A.J., Bergès, L., Bohner, A., Brooker, R. W., De Bruyn, L., De Cinti, B., Dirnböck, T., Grandin, U., Hester, A.J., Kanka, R., Klotz, S., Loucougaray, G., Lundin, L., Matteucci, G., Mészáros, I., Oláh, V., Preda, E., Prévosto, B., Pykälä, J., Schmidt, W., Taylor, M.E., Vadineanu, A., Waldmann, T., Stadler, J., 2011. Functional traits and local environment predict vegetation responses to disturbance: a pan-European multi-site experiment. J. Ecol. 99 (3), 777–787.
Beyth, M., 1972: The geology of central and western Tigre, Ethiopia. In Unpublished Ph. D. dissertation, University of Bonn, Germany.
Bigham, J.M., Fitzpatrick, R.W., Schulze, D.G., 2002. Iron oxides. Soil mineralogy with environmental applications 7, 323–366.
Blumfield, T.J., Xu, Z.H., Chen, C., 2005. Mineral nitrogen dynamics following soil compaction and cultivation during hoop pine plantation establishment. For. Ecol. Manage. 204 (1), 131–137.
Boardman, J., 2013. The hydrological role of 'sunken lanes' with respect to sediment mobilization and delivery to watercourses with particular reference to West Sussex, southern England. J Soils Sediments 13 (9), 1636–1644.
Bresson, L.M., Zambaux, C., 1990. Micromorphological study of compaction induced by mechanical stress for a Dystrochreptic Fragiudalf. In : Developments in soil science, vol. 19, Elsevier, pp. 33–40.
Breton, J.-F., 2011. Relations between Ethiopia and South Arabia: problems of architecture. Annales d'Éthiopie 26 (1), 53–77.
Buchwał, A.G.A.T.A., Rogowski, M.A.T.E.U.S.Z., 2010. The methods of preventing trail erosion on the examples of intensively used footpaths in the Tatra and the Babia Góra National Parks. Geomorphologia Slovaca et Bohemica 10 (1), 7–15.
Busch, R., Hardt, J., Nir, N., Schütt, B., 2021. Modeling gully erosion susceptibility to evaluate human impact on local landscape dynamics in Tigray, Ethiopia. Remote Sensing 13 (7).
Butzer, K.W., 2005. Environmental history in the Mediterranean world: cross-disciplinary investigation of cause-and-effect for degradation and soil erosion. J. Archaeol. Sci. 32 (12), 1773–1800. https://doi.org/10.1016/j.jas.2005.06.001.
Cao, L., Wang, Y.i., Li, Y.u., Li, X., 2021. Variations in rill morphology on unpaved road surfaces and their controlling factors. Earth Surf. Process. Landforms 46 (8), 1586–1599.
Chen, C., Hall, S.J., Coward, E., Thompson, A., 2020. Iron-mediated organic matter decomposition in humid soils can counteract protection. NatureCommunications 11 (1), 1–13.
Cole, D.N., 2004. Impacts of hiking and camping on soils and vegetation: a review. In: Buckley, R. (Ed.), Environmental impacts of ecotourism. CABI, Wallingford, pp. 41–60.
Contenson, Henri de, 1961. Les fouilles à Haoulti-Melazo en 1958. In *Annales d'Éthiopie* 4 (1), 39–60.
Coulon, E., Bruand, A., 1989. Effects of compaction on the pore space geometry in sandy soils. Soil Tillage Res. 15 (1–2), 137–151. https://doi.org/10.1016/0167-1987(89)90070-6.
Coward, E.K., Thompson, A.T., Plante, A.F., 2017. Iron-mediated mineralogical control of organic matter accumulation in tropical soils. Geoderma 306, 206–216. https://doi.org/10.1016/j.geoderma.2017.07.026.
Dagnew, D.C., Guzman, C.D., Zegeye, A.D., Tibebu, T.Y., Getaneh, M., Abate, S., Zemale, F.A., Ayana, E.K., Tilahun, S.A., Steenhuis, T.S., 2015. Impact of conservation practices on runoff and soil loss in the sub-humid Ethiopian Highlands: The Debre Mawi watershed. Journal of Hydrology and Hydromechanics 63 (3), 210–219.
David, L., Ilyes, Z., Baros, Z., 2011. Geological and geomorphological problems caused by transportation and industry. Open Geosciences 3 (3), 271–286.
Drauschke, Thomas, Oertel, Cornelius, Zurba, Kamal, Matschullat, Jörg, 2015. CO2-emissions from a short rotation forestry and a spruce forest site in the Erzgebirge, Germany. ББК *28.081+ 20.1 П 78*, p. 158.
Fattovich, Rodolfo, 2010. The development of ancient states in the northern Horn of Africa, c. 3000 BC–AD 1000: an archaeological outline. Journal of World Prehistory 23(3), 145–175.
Frankl, A., Poesen, J., Haile, M., Deckers, J., Nyssen, J., 2013. Quantifying long-term changes in gully networks and volumes in dryland environments: The case of Northern Ethiopia. Geomorphology 201, 254–263.
García, J.-L., Lüthgens, C., Vega, R.M., Rodés, Á., Hein, A., Binnie, S., 2021. A composite 10Be, IR-50 and 14C chronology of the pre-LGM full ice extent of the western Patagonian Ice Sheet in the Isla de Chiloé, south Chile (42°S. E&G-Quaternary Science Journal 70 (1).
Gebrehiwot, T., van der Veen, A., 2013. Assessing the evidence of climate variability in the northern part of Ethiopia. Journal of Development and Agricultural Economics 5 (3), 104–119.
Geeter, Sofie de; Poesen, Jean; Vanmaercke, Matthias, 2020. Does the topographic threshold concept explain the initiation points of sunken lanes in the European loess belt? CATENA 192, 104586.
Goldberg, P., Berna, F., 2010. Micromorphology and context. Quat. Int. 214 (1–2), 56–62.
Guimarães, D.V., Gonzaga, M.I.S., da Silva, T.O., da Silva, T.L., da Silva Dias, N., Matias, M.I.S., 2013. Soil organic matter pools and carbon fractions in soil under different land uses. Soil Tillage Res. 126, 177–182.
Harrower, M.J., Nathan, S., Mazzariello, J.C., Zerue, K., Dumitru, I.A., Meresa, Y., Bongers, J.L., Gebreegziabher, G., Zaitchik, B.F., Anderson, M.C., 2020. Water, Geography, and Aksumite Civilization: The Southern Red Sea Archaeological Histories (SRSAH) Project Survey (2009–2016). Afr. Archaeol. Rev. 37 (1), 51–67.
Hoelzmann, P., Klein, T., Kutz, F., Schütt, B., 2017. A new device to mount portable energy-dispersive X-ray fluorescence spectrometers (p-ED-XRF) for semi-continuous analyses of split (sediment) cores and solid samples. Geosci. Instrum. Methods Data Syst. 6 (1), 93–101.
Iraj, Bagheri; Samira Bahram, Kalhori; Mehdi, Akef; Farhad, Khormali, 2011. Effect of compaction on physical and micromorphological properties of forest soils. In *AJPS* 2012.
Jammalamadaka, S. Rao, Sengupta, Ambar, 2001. Topics in circular statistics: world scientific (5).
Jim, C.Y., 1993. Soil Compaction as a Constraint to Tree Growth in Tropical & Subtropical Urban Habitats. Envir. Conserv. 20 (1), 35–49. https://doi.org/10.1017/S0376892900037206.
Kaiser, K., Eusterhues, K., Rumpel, C., Guggenberger, G., Kögel-Knabner, I., 2002. Stabilization of organic matter by soil minerals—investigations of density and particle-size fractions from two acid forest soils. J. Plant Nutr. Soil Sci. 165 (4), 451–459.
Kawahigashi, M., Kaiser, K., Rodionov, A., Guggenberger, G., 2006. Sorption of dissolved organic matter by mineral soils of the Siberian forest tundra. Glob. Change Biol. 12 (10), 1868–1877.
Kilbride, C., Poole, J., Hutchings, T.R., 2006. A comparison of Cu, Pb, As, Cd, Zn, Fe, Ni and Mn determined by acid extraction/ICP–OES and ex situ field portable X-ray fluorescence analyses. Environ. Pollut. 143 (1), 16–23.
Kirsten, F., Fülling, A., Heinrich, S., Schneider, B., Heinrich, J., 2021. Early Holocene aeolian sediments in southwestern Crete—preliminary results. Med. Geosc. Rev. 3 (2), 269–287.
Kissling, M., Hegetschweiler, K.T., Rusterholz, H.-P., Baur, B., 2009. Short-term and long-term effects of human trampling on above-ground vegetation, soil density, soil organic matter and soil microbial processes in suburban beech forests. Appl. Soil Ecol. 42 (3), 303–314.
Leclant, J., 1959. Haoulti-Melazo (1955–1956). ethio 3 (1), 43–82. https://doi.org/10.3406/ethio.1959.1300.
Leopold, Luna B., Wolman, M. Gordon, Miller, John P., Wohl, Ellen, 2020. Fluvial processes in geomorphology: Courier Dover Publications.
Machado, Maria J., 2015. Geomorphology of the Adwa District. In : Landscapes and Landforms of Ethiopia, Springer, pp. 163–178.
Mikutta, R., Kleber, M., Torn, M.S., Jahn, R., 2006. Stabilization of soil organic matter: association with minerals or chemical recalcitrance? Biogeochemistry 77 (1), 25–56.
Miller, Christopher E., Conard, Nicholas J., Goldberg, Paul, Berna, Francesco, 2010. Dumping, sweeping and trampling: experimental micromorphological analysis of anthropogenically modified combustion features.
Mussi, Margherita, Altamura, Flavio, Di Bianco, Luca, Bonnefille, Raymonde, Gaudzinski-Windheuser, Sabine, Geraads, Denis et al., 2021. After the emergence of the Acheulean at Melka Kunture (Upper Awash, Ethiopia): From Gombore IB (1.6 Ma) to Gombore Iγ (1.4 Ma), Gombore Iδ (1.3 Ma) and Gombore II OAM Test Pit C (1.2 Ma). Quaternary International.
Nawaz, M.F., Bourrié, G., Trolard, F., Ranger, J., Gul, S., Niazi, N.K., 2016. Early detection of the effects of compaction in forested soils: evidence from selective extraction techniques. J. Soils Sediments 16 (9), 2223–2233.
Neve, S. de, Hofman, G., 2000. Influence of soil compaction on carbon and nitrogen mineralization of soil organic matter and crop residues. Biology and Fertility of Soils 30 (5-6), 544–549. DOI: 10.1007/s003740050034.
Nicosia, C., Stoops, G., 2017. Archaeological soil and sediment micromorphology. John Wiley & Sons.
Nir, Nadav, Knitter, Daniel, Hardt, Jacob, Schütt, Brigitta, 2021. Human movement and gully erosion: Investigating feedback mechanisms using Frequency Ratio and Least Cost Path analysis in Tigray, Ethiopia. PloS One 16 (2), e0245248.
Nykamp, Moritz, Knitter, Daniel, Schütt, Brigitta, 2020. Late Holocene geomorphodynamics in the vicinity of Göbekli Tepe, SE Turkey. CATENA 195, 104759.
Nyssen, J., Ghebreyohannes, T., Meaza, H., Dondeyne, S., 2020. Exploration of a medieval African map (Aksum, Ethiopia)–How do historical maps fit with topography?. In: Liber Amicorum: Philippe De Maeyer In Kaart. University Press, pp. 165–178.
Nyssen, J., Poesen, J., Haile, M., Moeyersons, J., Deckers, J., 2000. Tillage erosion on slopes with soil conservation structures in the Ethiopian highlands. Soil Tillage Res. 57 (3), 115–127.
Nyssen, J., Poesen, J., Moeyersons, J., Deckers, J., Haile, M., Lang, A., 2004. Human impact on the environment in the Ethiopian and Eritrean highlands—a state of the art. Earth Sci. Rev. 64 (3–4), 273–320. https://doi.org/10.1016/S0012-8252(03)00078-3.
Nyssen, J., Poesen, J., Moeyersons, J., Luyten, E., Veyret-Picot, M., Deckers, J., Haile, M., Govers, G., 2002. Impact of road building on gully erosion risk: a case study from the Northern Ethiopian Highlands. Earth Surf. Process. Landforms 27 (12), 1267–1283.
Pietola, L., Horn, R., Yli-Halla, M., 2005. Effects of trampling by cattle on the hydraulic and mechanical properties of soil. Soil Tillage Res. 82 (1), 99–108. https://doi.org/10.1016/j.still.2004.08.004.
Pires, L.F., Reichardt, K., Cooper, M., Cássaro, F.A.M., Dias, N.M.P., Bacchi, O.O.S., 2009. Pore system changes of damaged Brazilian oxisols and nitosols induced by wet-dry cycles as seen in 2-D micromorphologic image analysis. Anais da Academia Brasileira de Ciências 81 (1), 151–161.
QGIS.org, 2021. QGIS Geographic Information System: QGIS Association, 2021.
R Core Team, 2013. R: A language and environment for statistical computing.
Rasa, K., Eickhorst, T., Tippkötter, R., Yli-Halla, M., 2012. Structure and pore system in differently managed clayey surface soil as described by micromorphology and image analysis. In *Geoderma* 173–174, 10–18. https://doi.org/10.1016/j.geoderma.2011.12.017.

Rentzel, P., Nicosia, C., Gebhardt, A., Brönnimann, D., Pümpin, C., Ismail-Meyer, K., 2017. Trampling, poaching and the effect of traffic. In: Nicosia, C., Stoops, G. (Eds.), Archaeological Soil and Sediment Micromorphology. John Wiley & Sons, Ltd, Chichester, UK, pp. 281–297.

Rodgers, M.M., 1988. Dynamic biomechanics of the normal foot and ankle during walking and running. Physical Therapy 68 (12), 1822–1830.

Roovers, P., Verheyen, K., Hermy, M., Gulinck, H., 2004. Experimental trampling and vegetation recovery in some forest and heathland communities. Appl. Veg. Sci. 7 (1), 111–118. https://doi.org/10.1111/j.1654-109X.2004.tb00601.x.

Shahack-Gross, R., Marshall, F., Weiner, S., 2003. Geo-ethnoarchaeology of pastoral sites: the identification of livestock enclosures in abandoned Maasai settlements. J. Archaeol. Sci. 30 (4), 439–459.

Sherman, C., Unc, A., Doniger, T., Ehrlich, R., Steinberger, Y., 2019. The effect of human trampling activity on a soil microbial community at the Oulanka Natural Reserve, Finland. Appl. Soil Ecol. 135, 104–112.

Shipitalo, M.J., Nuutinen, V., Butt, K.R., 2004. Interaction of earthworm burrows and cracks in a clayey, subsurface-drained, soil. Appl. Soil Ecol. 26 (3), 209–217.

Sidle, Roy C., Jarihani, Ben, Gallant, John, Koci, Jack (Eds.), 2019. Evidence of how roads and trails contribute to gully erosion in drylands, 21.

Sidle, Roy C., Sasaki, Shozo, Otsuki, Mieko, Noguchi, Shoji, Rahim Nik, Abdul, 2004. Sediment pathways in a tropical forest: effects of logging roads and skid trails. Hydrological Processes 18 (4), 703–720.

Silva, S.R., Silva, I.R.d., Barros, N.F.d., Sá Mendonça, E.d., 2011. Effect of compaction on microbial activity and carbon and nitrogen transformations in two oxisols with different mineralogy. Rev. Bras. Ciênc. Solo 35 (4), 1141–1149.

Snead, James, Erickson, Clark L., Darling, Andrew, 2009. Making human space: the archaeology of trails, paths, and roads.

Stoops, G., 2021. Guidelines for analysis and description of soil and regolith thin sections, vol. 184. John Wiley & Sons.

Storozum, M.J., Goldstein, S.T., Contreras, D.A., Gidna, A.O., Mabulla, A.Z.P., Grillo, K. M., Prendergast, M.E., 2021. The influence of ancient herders on soil development at Luxmanda, Mbulu Plateau, Tanzania. CATENA 204, 105376. https://doi.org/10.1016/j.catena.2021.105376.

Tejedo, P., Benayas, J., Cajiao, D., Albertos, B., Lara, F., Pertierra, L.R., Andrés-Abellán, M., Wic, C., Luciáñez, M.J., Enríquez, N., Justel, A., Reck, G.K., 2016. Assessing environmental conditions of Antarctic footpaths to support management decisions. Journal of Environmental Management 177, 320–330.

Tichomirowa, M., Käßner, A., Sperner, B., Lapp, M., Leonhardt, D., Linnemann, U., Münker, C., Ovtcharova, M., Pfänder, J.A., Schaltegger, U., Sergeev, S., von Quadt, A., Whitehouse, M., 2019. Dating multiply overprinted granites: The effect of protracted magmatism and fluid flow on dating systems (zircon U-Pb: SHRIMP/SIMS, LA-ICP-MS, CA-ID-TIMS; and Rb–Sr, Ar–Ar)–Granites from the Western Erzgebirge (Bohemian Massif, Germany). Chem. Geol. 519, 11–38.

Umweltamt Steglitz-Zehlendorf von Berlin, 2016. Wasserbuch Steglitz-Zehlendorf (Memento des Originals vom 13. Januar 2016 im Internet Archive). Umweltamt Steglitz-Zehlendorf von Berlin.

USGS: United States Geological Survey (USGS) Earth Explorer. Available online at https://earthexplorer.usgs.gov.

Valentin, C., Poesen, J., Li, Y., 2005. Gully erosion: Impacts, factors and control. CATENA 63 (2–3), 132–153.

van Andel, T.H., Zangger, E., Demitrack, A., 1990. Land Use and Soil Erosion in Prehistoric and Historical Greece. Journal of Field Archaeology 17 (4), 379–396. https://doi.org/10.2307/530002.

Vandaele, K., Poesen, J., Govers, G., van Wesemael, B., 1996. Geomorphic threshold conditions for ephemeral gully incision. Geomorphology 16 (2), 161–173.

Verhagen, P., Nuninger, L., Groenhuijzen, M.R., 2019. Modelling of pathways and movement networks in archaeology: an overview of current approaches. In: Finding the Limits of the Limes, pp. 217–249.

Verrecchia, Eric P., 2021. A Visual Atlas for Soil Micromorphologists: Springer Nature. Available online at https://link.springer.com/book/10.1007/978-3-030-67806-7?fbclid=IwAR1582LYAVCrbad0T_o1BZVY6ZOacVh4DSOv6msjSlgEpWt9MaoQon3M8M0&s=09.

Wang, D., Blumfield, T.J., Xu, Z., 2020. Long-term impacts of soil compaction and cultivation on soil carbon and nitrogen pools, foliar δ13C and δ15N as well as tree growth in a hoop pine plantation of subtropical Australia. J. Soils Sediments 20 (7), 2829–2842. https://doi.org/10.1007/s11368-020-02654-8.

Weiß, C.h., Köster, M., Japp, S., 2016. Preliminary characterization of pottery by cathodoluminescence and SEM–EDX analyses: an example from the Yeha region (Ethiopia). Archaeometry 58 (2), 239–254.

Wessolek, G., Schwärzel, K., Greiffenhagen, A., Stoffregen, H., 2008. Percolation characteristics of a water-repellent sandy forest soil. Eur. J. Soil Sci. 59 (1), 14–23.

Wimpey, J.F., Marion, J.L., 2010. The influence of use, environmental and managerial factors on the width of recreational trails. J. Environ. Manage. 91 (10), 2028–2037.

Yaşar Korkanç, Selma, 2014. Impacts of recreational human trampling on selected soil and vegetation properties of Aladag Natural Park, Turkey. CATENA 113, pp. 219–225. DOI: 10.1016/j.catena.2013.08.001.

Zedeño, María Nieves; Stoffle, Richard W., 2003. Tracking the role of pathways in the evolution of a human landscape: the St. Croix Riverway in ethnohistorical perspective. Colonization of unfamiliar landscapes: the archaeology of adaptation, pp. 59–80.

Zgłobicki, W., Poesen, J., De Geeter, S., Boardman, J., Gawrysiak, L., Golosov, V., Ionita, I., Niacsu, L., Rodzik, J., Stankoviansky, M., Stolz, C., 2021. Sunken lanes - Development and functions in landscapes. Earth Sci. Rev. 221, 103757.

Ziegler, A.D., Sutherland, R.A., Giambelluca, T.W., 2000. Runoff generation and sediment production on unpaved roads, footpaths and agricultural land surfaces in northern Thailand. Earth Surf. Process. Landforms 25 (5), 519–534.